

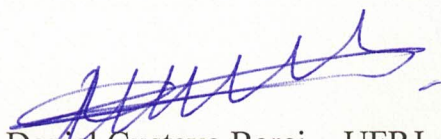
"PURIFICATION OF A CONTINUOUSLY MEASURED QUBIT"

**MATHEUS MONTEIRO RAMALHO POLTRONIERI MARTINS**

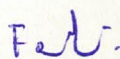
Dissertação de Mestrado em Física apresentada no  
Centro Brasileiro de Pesquisas Físicas do  
Ministério da Ciência Tecnologia e Inovação.  
Fazendo parte da banca examinadora os seguintes  
professores:



Tobias Micklitz - Orientador/CBPF



Daniel Gustavo Barci - UFRJ



Fernando Iemini de Rezende Aguiar – UFSJ

Rio de Janeiro, 02 de setembro de 2024.



Centro Brasileiro de Pesquisas Físicas

Coordenação de Física Teórica - COTEO

# Purification of a continuously measured qubit

Aluno: Matheus Monteiro Ramalho Poltronieri Martins

Orientador: Tobias Micklitz

Rio de Janeiro-RJ  
2024

# Agradecimentos

Aos meus pais, Claudson e Ana Lúcia, por todo o apoio e incentivo que me deram para chegar aqui.

A minha esposa Ana Luiza, pelo carinho e apoio, e que me incentiva a crescer como pessoa a cada dia; e a nossa filha Olivia, cuja presença neste mundo é motivo de grande alegria para mim.

Ao meu tio Alan, cujas discussões e visitas aos laboratórios da UENF despertaram o meu interesse científico.

A minha família, por me apoiarem direta ou indiretamente em minha formação acadêmica, mas sobretudo como pessoa.

Aos colegas e amigos do CBPF, cuja amizade e companheirismo surgiram como um sopro de vida nesses anos.

Ao Piero, grande amigo que fiz no mestrado, cuja companhia e senso de humor foram um grande alento nesse dois anos de mestrado.

Ao meu orientador Tobias, por compartilhar sua experiência e conhecimento sobre física da matéria condensada e por sua orientação durante o mestrado.

E, por fim, à Coordenação de Aperfeiçoamento de Pessoal de Nível Superior (CAPES), pelo apoio e incentivo à pesquisa.

## Resumo

Investigamos a distribuição da puridade, entropia de Von-Neumann e do ganho de informação a partir da medição contínua de um único qubit. A medição contínua no tempo é realizada acoplando um único qubit a qubits auxiliares que são medidos projetivamente a uma taxa constante. Partindo de uma equação mestra estocástica que descreve a evolução efetiva do qubit, este último é mapeado numa equação de Langevin com ruído multiplicativo. Esta equação é resolvida em termos de uma integral de caminho de Onsager-Machlup, a partir da qual calculamos a distribuição de probabilidade dos observáveis de interesse após medição contínua por um tempo  $t$ . Em específico, a distribuição de probabilidade do ganho de informação evolui de uma função fortemente concentrada em torno da informação 0 em curtos períodos de tempo para uma função fortemente concentrada em torno da informação 1 para longos períodos de tempo, passando por uma estrutura de dois picos em períodos intermediários. Testamos nossas descobertas analíticas por meio de simulações numéricas e encontramos excelente concordância.

**Palavras-chave:** Trajetórias quânticas, Equação de Langevin, integral de caminho de Onsager-Machlup, ganho de informação.

## Abstract

We investigate the distribution of the purity, Von-Neumann entropy, and information gained from continuously measuring a single qubit. The continuous-in-time measurement is realized by coupling the single qubit to ancillary qubits which are projectively measured at a constant rate. Starting from a stochastic master equation that accounts for an effective evolution of the single qubit, the latter is mapped to a Langevin equation with multiplicative noise. This equation is solved in terms of an Onsager-Machlup path integral, from which we calculate the probability distribution of observables of interest after continuously measuring for a time  $t$ . In particular, the probability distribution of the information gain evolves from a function sharply peaked at information 0 at short times into a function sharply peaked at information 1 at long times, via a two-peak structure at intermediate times. We test our analytic findings by numerical simulations and find excellent agreement.

**Keywords:** Quantum trajectories, Langevin's equation, Onsager-Machlup path integral, information gain.

# Contents

<b>Agradecimientos</b>	<b>1</b>
<b>1 Introduction</b>	<b>2</b>
1.1 Measurement-induced phase transition in hybrid dynamics	3
1.2 Extreme regimes of purification dynamics	6
1.3 Problem statement and overview	7
<b>2 Non-unitary diffusion quantum trajectory of a single qubit</b>	<b>10</b>
2.1 Stochastic Schrodinger Equation (SSE)	11
2.2 Stochastic Master Equation (SME)	17
2.3 Langevin equation of non-unitary diffusion quantum trajectories	18
<b>3 Quantum trajectories numerical simulation</b>	<b>20</b>
3.1 Method	20
3.2 Non-unitary diffusion quantum trajectories	22
3.3 Observables of interest	24
3.3.1 Purity	25
3.3.2 Von-Neumann entropy and information gain	27
<b>4 Exact solution for quantum trajectories probability distribution</b>	<b>31</b>
4.1 Stratonovich Langevin equation without multiplicative noise	33
4.2 Path probability distribution	35
4.3 Saddle point solution	39
<b>5 Comparison with numerical results</b>	<b>44</b>
5.1 Probability distributions	44
5.2 Averages and fluctuations	47
<b>6 Conclusions</b>	<b>49</b>
<b>A Non-unitary diffusion Master Equation using POVM's</b>	<b>51</b>
<b>B Basic notions of Stochastic calculus</b>	<b>53</b>
B.1 Discrete-time stochastic differential equation and Itô's rule	54
B.2 Change of discretization	55
B.3 The stochastic chain rule	57
B.4 Change of variable in Langevin equation	58

# Chapter 1

## Introduction

In quantum mechanical systems, there are two types of dynamics: unitary evolution and measurements. Unitary gates applied between different particles tend to grow entanglement between them. As a result, initially localized information is scrambled because of the correlations introduced throughout the sample. Conversely, when we measure a particle through projective operators, its state is revealed at the expense of the loss of quantum coherence. Therefore, the measured particle inevitably became uncorrelated from the rest of the sample, and overall entanglement is reduced in the process [1].

In a hybrid quantum circuit, both of these processes take place. Therefore, the dynamics of a hybrid system are characterized by a competition between the growth and the decline of entanglement. Hybrid circuits have been widely studied in condensed matter physics to probe universal features of far-from-equilibrium quantum systems. One intriguing problem where entanglement plays a key role, for example, is to define when a many-body quantum system thermalizes and when it does not. For a highly entangled state, the subsystem density matrix has a Gibbs distribution, obeying the conditions of the Eigenstate-Thermalization Hypothesis (ETH) [2, 3, 4]. In this case, the system acts as a thermal bath for itself, and only global thermodynamical information is accessible; local information is scrambled throughout the sample due to long-range entanglement [5, 6, 7, 8, 9]. In contrast, for many-body localized systems, information scrambling is inhibited by strong disorder or by measurements [10, 11]. In this case, entanglement is localized within a subsystem, while subsystems very distant from one another (distance of the order of the sample size) remain uncorrelated. Therefore, a system with many-body localization will exhibit non-trivial properties at large times, i.e., it will not thermalize,

keeping the memory of its initial state [12, 10].

## 1.1 Measurement-induced phase transition in hybrid dynamics

In particular, it was recently discovered that monitored hybrid quantum circuits would exhibit a measurement-induced phase transition from an ergodic to a many-body localized phase [13, 14, 15]. For example, consider the following 1+1D, quantum circuit:

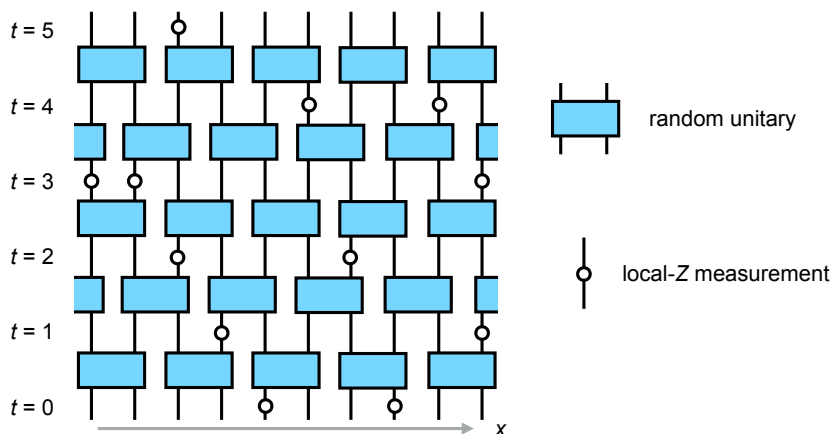


**Figure 1.1:** A hybrid 1+1D quantum circuit with  $L = 10$  qubits. At each time step, local measurement is performed with probability  $p$ . Between time steps, local random unitary gates act between neighboring qubits, alternating the neighbor between layers. Image from Ref. [16]

Starting in a pure state  $|\Psi\rangle = \prod_n |0\rangle^{\otimes n}$ , local random unitary gates will tend to grow overall entanglement of the sample, while local measurements that project the qubit into the  $z$  component, occurring with probability  $p$ , disentangle the measured qubit with its neighbors (see Fig. 1.1). The taming of entanglement can be tuned by the single parameter  $p$ , which modulates the measurement frequency. The amount of entanglement in the sample can be quantified by the reduced Renyi entropy  $S_A^n$ :

$$S_A^n = \frac{1}{1-n} \log_2 \text{tr} \rho_A^n,$$

where  $\rho_A = \text{tr}_{\bar{A}} |\Psi\rangle\langle\Psi|$  and  $(A, \bar{A})$  is an adjacent bipartition of the  $L$ -qubit system. The special case  $S_A^{n=1}$  reduces to the Von-Neumann entropy  $S_A = -\text{tr} \rho_A \log_2 \rho_A$ . When  $p = 0$ , entanglement will grow to its maximum value limited by the sample size  $|A|$ . Therefore, the entanglement entropy averaged over many realizations of the random quantum circuit



will have a volume law scaling  $S_A \sim |A|$  at the steady state  $t \rightarrow \infty$ , with logarithmic correction at short times. Thus

$$S_A = \alpha \log |A| + s|A|,$$

for  $p = 0$ , where  $\alpha$  and  $s$  are constants. In [13], it is argued that any  $p \neq 0$  measurement rate will drive the system into an area law entropy  $S_A \propto |A|^0$ . However, numerical evidence from [15, 14] shows that volume law scaling of the entanglement entropy survives a measurement rate  $p < p_c$ , where  $p_c$  is a critical threshold above which one obtains area-law behavior. At the critical measurement rate  $p = p_c$ , the entanglement entropy has a logarithmic dependence on the subsystem size [15, 16]:

$$S_A = \alpha(p_c) \log |A|.$$

The behavior of the averaged entanglement entropy probed by simulation is summarized in Fig. 1.2 below:

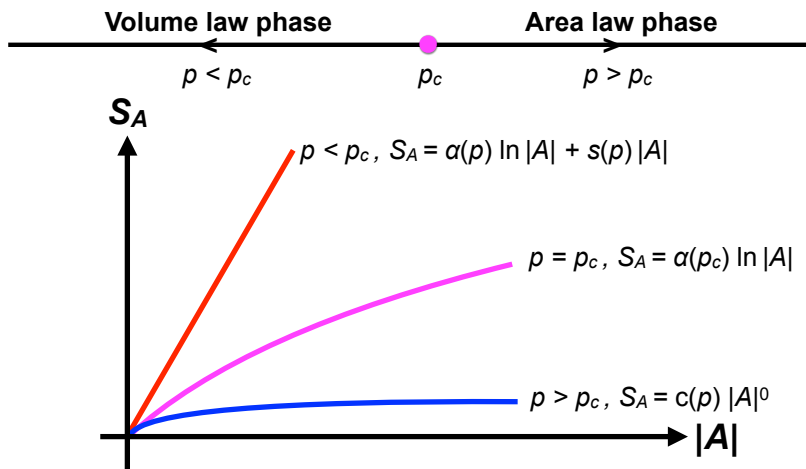


**Figure 1.2:** Entanglement entropy,  $S_A$ , averaged over many realizations of the hybrid model illustrated in Fig. 1.1. A measurement rate threshold  $p_c$  separates a volume law entanglement phase ( $p < p_c$ ) from an area-law phase ( $p > p_c$ ). At the critical point, the entanglement entropy has a pure logarithmic behavior, resulting from scale invariance. Figure taken from Ref. [16].

At the critical point, the mutual information  $I_{A,B}^n = S_A^n + S_B^n - S_{AUB}^n$  between two spins distant by  $x \gg 1$  obey a power law scaling  $I^n(x) \sim x^{-2\Delta_c}$ , where  $\Delta_c \approx 2$ , with exponential decay away from criticality [15, 16]. These results point to an underlying conformal field theory (CFT) describing this phase transition. This connection motivated an analytical description using tensor network holography [17].

An analytical solution for the Hartley entropy  $S_A^{n=0} = \log(\text{rank}(\rho_A))$  is accessible for

the 1+1D case by an exact mapping [18] between quantum hybrid circuits and classical percolation [19, 20, 21]. This mapping between the two problems can be seen in Fig. 1.3 below:

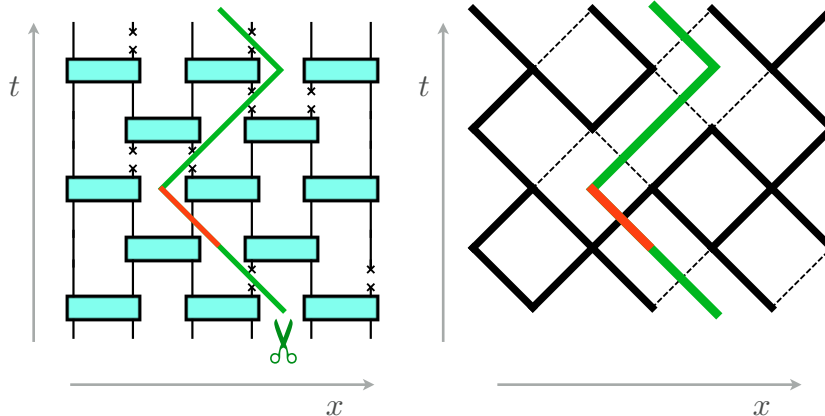


**Figure 1.3:** (Left) A hybrid quantum circuit with a minimal cut configuration (green line). (Right) Mapping of the hybrid circuit with classical percolation theory. Each two qubits unitary became a point in the percolation graph. A bond between these points occurs with probability  $1 - p$ . Therefore, a measurement breaks a bond in the percolation network. Whenever the minimal cut crosses a bond, it has a cost, summing one value to the Hartley entropy. Crossing a broken bond does not cost anything, and the entropy keeps a constant value. The figure is taken from [15]

The exact calculation for the Hartley entropy is performed by calculating the minimal cut configuration for the lattice percolation [15]. Using this method, it was found that  $p_c = \frac{1}{2}$  and the correlation length near the critical point behaves as  $\xi \sim |p - p_c|^{-\nu}$ , with  $\nu = \frac{4}{3}$  [15]. While more generic cases do not allow an exact description, the phase transition still exists, but with other critical exponents and other values for  $p_c$  [15, 14, 16].

Finally, the assumptions of random unitary interaction between neighbors and projective measurements are not necessary for the existence of the measured-induced phase transition. They can be relaxed by considering Floquet dynamics with Clifford gates [22], for example, or weak measurements instead of projective ones [23], without qualitatively altering the results: a phase transition would still occur for a finite threshold of the measurement rate, dividing volume law to area law behavior of the entanglement entropy.

## 1.2 Extreme regimes of purification dynamics

In a monitored many-body quantum system, we can distinguish two extreme cases for the system purification behavior: a *strong* and a *weak* measurement regime, respectively. Let  $J$  be the typical energy of interaction of an all-to-all interacting many-body system and  $\eta$  be the measurement rate under which the system is probed. A *weak measurement* regime occurs when  $\eta \ll J$ , that is when the measurement rate is much smaller than the relaxation time to ergodicity. In this case, between any two measurements, the system will be ergodic. Therefore, the quantum circuit that characterizes this phase can be described by layers of random distributed projective measurements, with all-to-all Haar random unitaries acting between those layers. Starting in a mixed state, it was found the following analytical expression for the mean purity  $\langle \tau \rangle = \langle \text{tr } \rho^2 \rangle$  of  $N$  qubits, with the average calculated over many copies of the initial state [24]:

$$\langle \tau_t \rangle \approx \frac{\sinh(t/t_p) + D^{-1} \cosh(t/t_p)}{\cosh(t/t_p) + D^{-1} \sinh(t/t_p)}, \quad (1.1)$$

where  $D = 2^N$  is the Hilbert space dimension and  $t_p = D/N\eta$  is the typical purification time, which grows exponentially with the number  $N$  of particles.

In contrast, the strong measurement regime occurs when  $\eta \gg J$ . In this case, the time interval between measurements is so small compared to the scrambling time, that the system has no time to undergo relaxation under its dynamics. Therefore, interaction can be disregarded altogether. In this limiting case, the analysis is simplified by random measurement distributed by a Poisson process, with the probability for a single qubit of the sample to be projectively measured being  $p = 1 - e^{-\eta t}$ . Therefore, the mean purity evolution of a single qubit will be:

$$\langle \tau_1 \rangle = e^{-\eta t} \times \frac{1}{2} + (1 - e^{-\eta t}) \times 1 = 1 - \frac{1}{2}e^{-\eta t}. \quad (1.2)$$

Whereas for  $N$  non-interacting qubit, we have:

$$\langle \tau \rangle = \prod_{n=1}^N \langle \tau_1 \rangle = \left( 1 - \frac{1}{2}e^{-\eta t} \right)^N. \quad (1.3)$$

The typical purification time in this case grows logarithmically with the number of particles by  $t_p = \eta^{-1} \ln N$  [24].

Comparison between the analytical expressions from Eq. (1.1) and Eq. (1.3) and the

respective quantum circuit simulation for  $\eta = 1/N$  (uniform distribution throughout the sample) can be seen in the Fig. 1.4 below:

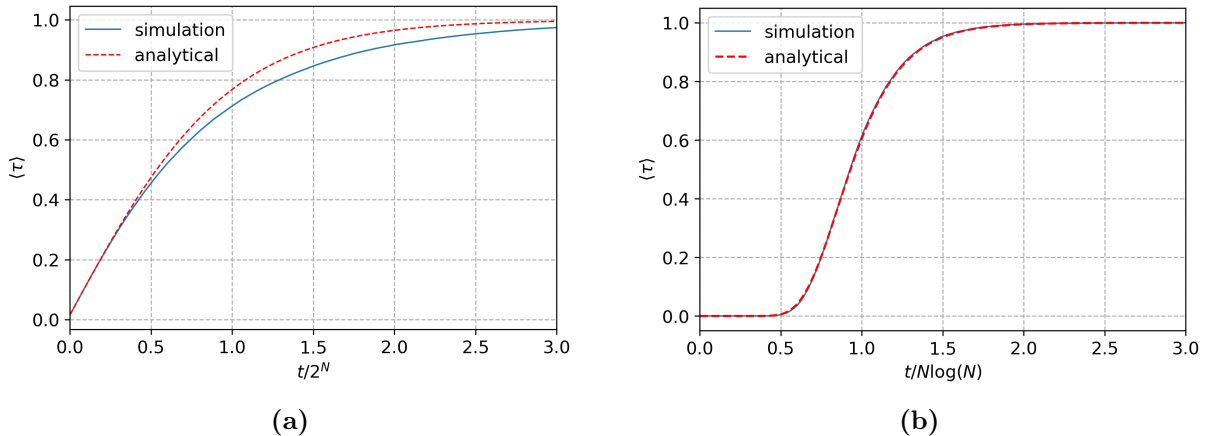


**Figure 1.4:** Mean purity  $\langle \tau \rangle = \langle \text{tr } \rho^2 \rangle$  in the weak (left) and strong (right) measurement phase. Comparison with Eqs. (1.1) and (1.3) for  $N = 6$  and  $N = 100$ , respectively. Averages were calculated with 100,000 samples. Both cases start in a mixed state, therefore  $\langle \tau_0 \rangle = 1/D$ , where  $D = 2^N$ .

Although the analytic expression for the weak phase has the right asymptotic limit for small and large times (see [24] for more detailed analysis), it overestimates purification at intermediate times (see Fig. 1.4a). Conversely, in the thermodynamical limit where  $\frac{1}{N} \rightarrow 0$ , the strong measurement phase is exactly described by a Poisson process [24], as is clear from Fig. 1.4b.

### 1.3 Problem statement and overview

In the present work, we take a step back from the many-body problem and the hybrid dynamics and consider the case of a single qubit being continuously monitored in time. The purification of one qubit projectively measured would instantaneously jump from  $\tau = \frac{1}{2}$  to  $\tau = 1$  after measurement. In our case, this transition is made more gradual, since only a small amount of information is extracted in a small time interval, but now many measurements are required to fully purify a qubit (continuous monitoring). Our main goal is to find an analytical solution describing the purification of the continuously monitored qubit, in a similar way to what was achieved with Eq. (1.2) for the strong measurement regime. We will restrict our solution by considering only initial mixed states. As a result, the dynamics are greatly simplified, since only the time evolution of the diagonal elements has to be considered. Although at first, this seems a great constraint

for a realistic model it is quite the opposite, as for most systems, decoherence time is much smaller than the dynamical time of the system [25, 26]. So off-diagonal elements can be disregarded without great loss of generality.

Contrary to the many-body problem, where non-trivial phases are tuned by the measurement rate, the continuously monitored qubit always ends up being purified (a pure state is reached at the end of the process). Despite the differences between the simplified model studied in this thesis and the many-body case, we think the task of studying the continuously monitored qubit is justifiable. The first reason is the validation of the Feynman-path integral method for the non-unitary diffusion of a qubit under monitoring. Secondly, by using this method, we were able to find an exact expression for the probability distribution of the entropy and the gain of information of the continuously monitored qubit.

To reach our objectives, this thesis is divided in the following way: In Chapter 2 we deduce the dynamical equation of the continuously monitored qubit for the wave function (Stochastic Schrodinger equation) and the density matrix (Stochastic Master equation). Next, we show that the purification of a mixed state can be described by one degree of freedom obeying a Langevin equation with multiplicative noise. In Chapter 3, by mean of the Langevin equation obtained, we numerically simulate the quantum trajectories, either individually for the states, or averages for observables that quantify purification, like the purity, the Von-Neumann entropy, and the information gained by measurements. From the individual trajectories, we were also able to simulate the probability distributions of the observables. All calculations were done using the Euler-Maruyama method [27] to numerically integrate the Langevin equation. In Chapter 4, we formally build the probability distribution for the trajectories of the Langevin equation. This probability distribution is constructed using the Onsager-Machlup approach [28, 29] discretized at the midpoint (Stratonovich) for an equivalent stochastic evolution with additive noise. We then find a saddle-point solution for the probability distribution calculated and compare it with our numerical findings for the purity, obtaining excellent agreement. In Chapter 5, we compare the prediction given by our analytical solution with the results obtained numerically in Chapter 3, such as the probability distributions, expected values, and variances for the quantum trajectories, purity, entropy, and information gain. Again, excellent agreement is found in every case. Finally, in chapter 5 we give a brief outline

of what was achieved. We present the main findings and give some ideas for future development of the present work.

## Chapter 2

# Non-unitary diffusion quantum trajectory of a single qubit

Measurement in quantum mechanics is usually presented by employing projective operators that instantaneously extract full information about the probed system. Although this theory is successful in many ways [30], it fails to describe situations where the quantum nature of the measurement process has to be taken into account, such as in quantum optics. For example, to probe a Rydberg atom (an atom possessing two accessible electronic states.), one does not measure it directly using a supposed 'energy level' detector. In practice, measurements are indirectly conducted by directing an electromagnetic field, made up of photons, toward the atom. The incident photon will weakly interact with the atom, carrying partial information about its electronic state with it. Then the probing photon will be measured by a photodetector. Because the weak interaction introduced a small correlation between the photon and the atom, knowledge of the photon state will reveal partial information about the atom's electronic state. By probing the atom with radiation at a constant rate, the atom state is conditioned by the (indirect) measurement outcomes from the photodetector. As a result, the atom state will be effectively described by a non-linear stochastic differential equation describing a path conditioned by the experiment outcomes, that is, a *quantum trajectory* ([31, 32, 33, 34, 35, 36]). The non-linearity arises because the system state has to be renormalized after every step to keep its norm equal to one; while the randomness effectively describes the measurement outcomes of the subsystem.

More generally, a quantum trajectory is obtained by coupling the system to an envi-

ronment that is subsequently monitored [35]. The effective description of the system will result in a stochastic Schrödinger equation for the system state or a Stochastic Master equation for its density matrix. The nature of this stochastic time evolution will depend on the environment state and the interaction between the system and the environment. When describing the spontaneous emission of an atom, these trajectories evolve deterministically in a non-unitary manner, until a discontinuous event occurs at random for the trajectory, which signals that the emission has occurred [37, 35, 33]; this case is commonly referred as the *quantum jump* method, because of its discontinuous nature. In this chapter, we will consider the case of non-unitary diffusion. In this evolution, starting, for example, in a (diagonal) mixed state, half of the time the system will be purified into the state  $|0\rangle\langle 0|$  and half of the time into the state  $|1\rangle\langle 1|$ , with a diffusive behavior of the system state at intermediate times. The diffusion decreases to zero as the system approaches the pure states  $|0\rangle$  or  $|1\rangle$ , and stops entirely once either of these pure states is reached. Therefore, this case can be seen as an indirect measurement of the qubits  $|0\rangle$  or  $|1\rangle$ , recovering the projective measurement prediction in the limit  $t \rightarrow \infty$ . For further details on the reasoning shown in this chapter, we refer to [35].

## 2.1 Stochastic Schrodinger Equation (SSE)

To perform a weak measurement over a qubit in a general state  $|\psi\rangle = \alpha|0\rangle + \beta|1\rangle$  (system), we first weakly couple it with another probing qubit in a state  $|\phi\rangle$  (ancilla). This coupling is performed by a unitary (weak) interaction  $U$ . A projective measurement is then performed in the ancilla, with two possible outcomes. The process is then repeated at every time interval  $dt$ . A schematic representation of the model is in Fig. 2.1



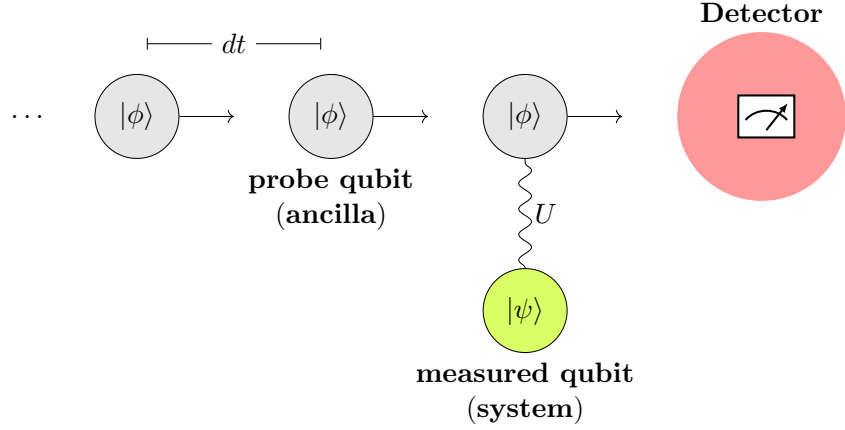


**Figure 2.1:** Schematic representation of the collisional model used to deduce the Stochastic Schrödinger Equation. The measured qubit (system) interacts with the probing qubit in the ancilla via the unitary operator  $U$ . Subsequently, the ancilla qubit is measured, revealing partial information about the system, and traced out. Effectively, at every interval  $dt$ , a weak measurement will be performed on the system. Note that all ancillary qubits are prepared in the same state  $|\phi\rangle$ , and the system interacts with one ancillary qubit at a time. These conditions are met for a Markovian time evolution of the system [38].

Because of the small entanglement introduced by  $U$  between the two subsystems, the measurement over the ancilla will provide a small amount of information about the state  $|\psi\rangle$ . As a consequence, the system will change by  $|\psi\rangle \rightarrow |\psi\rangle + d|\psi\rangle$ . The nature of this change depends on the ancilla state  $|\phi\rangle$  and the coupling  $U$  between subsystems, leading to different qubit measurement schemes [35, 33]. For the non-unitary diffusion case, the ancilla qubits are prepared in the state

$$|\phi\rangle \equiv |y_{-}\rangle = (|0\rangle - i|1\rangle)/\sqrt{2},$$

while the interaction between the system and the ancillary qubits is intermediated by the unitary operator

$$U = Z_S(\theta)U_{\text{CNOT}}(\theta),$$

where

$$U_{\text{CNOT}}(\theta) = e^{-i\theta\text{CNOT}} = \cos\theta - i\text{CNOT}\sin\theta,$$

and  $Z_S(\theta) = e^{i\theta\sigma_z/2} \otimes \hat{1}$  [35]. The CNOT operator, pronounced as Controlled-Not, is a two-qubit operator conditioned on a control qubit. It works by applying the operator  $\sigma_1^*$  over the second qubit when the first qubit is equal to one. Otherwise, it acts as the

\*

$$\sigma_1 = \begin{pmatrix} 0 & 1 \\ 1 & 0 \end{pmatrix}$$

identity operator. This conditional behavior is summarized by the following equation:

$$\text{CNOT} = |0\rangle\langle 0| \otimes \hat{1} + |1\rangle\langle 1| \otimes \sigma_1.$$

▮ The parameter  $\theta$  modulates the coupling strength. To ensure continuous monitoring, we fix  $\theta = \sqrt{dt}$ , hence  $\theta \ll 1$  for an infinitesimal time interval  $dt$ . The total system (system + ancilla) is initially described by the state  $|\Psi\rangle = |\psi\rangle \otimes |\phi\rangle$ . After the interaction, the two-qubit state will change from  $|\Psi\rangle$  to  $|\Psi'\rangle = U|\Psi\rangle$ . Since  $\theta$  is a small parameter,  $U_{\text{CNOT}}(\theta)$  introduces a small entanglement between the two subsystems. Applying it to  $|\Psi\rangle$ , we obtain:

$$|\Psi''\rangle = U_{\text{CNOT}}(\theta)|\Psi\rangle = (\cos\theta - i\text{CNOT}\sin\theta)(\alpha|0y_-\rangle + \beta|1y_-\rangle).$$

Since  $\text{CNOT}|0y_-\rangle = |0y_-\rangle$  and  $\text{CNOT}|1y_-\rangle = -i|1y_+\rangle$ , where  $|y_{\pm}\rangle = (|0\rangle \pm i|1\rangle)/\sqrt{2}$ , we have that:

$$|\Psi''\rangle = (\alpha e^{-i\theta}|0\rangle + \beta \cos\theta|1\rangle) \otimes |y_-\rangle - \beta \sin\theta|1\rangle \otimes |y_+\rangle.$$

To eliminate the relative phase factor  $e^{-i\theta}$  between the system components coupled to  $|y_-\rangle$ , we apply  $Z_S(\theta) = e^{i\theta\sigma_z/2} \otimes \hat{1}$  to  $|\Psi''\rangle$ . This operation does not affect the effective behavior of the system qubit, since no correlation between subsystems is introduced. The result is, apart from an overall phase factor  $e^{-i\theta/2}$ :

$$|\Psi'\rangle = (\alpha|0\rangle + \beta \cos\theta|1\rangle) \otimes |y_-\rangle - \beta \sin\theta|1\rangle \otimes |y_+\rangle.$$

Expanding the states  $|y_{\pm}\rangle$  into the computational basis, we obtain:

$$|\Psi'\rangle = |s_0\rangle \otimes |0\rangle - i|s_1\rangle \otimes |1\rangle,$$

where

$$\begin{aligned} |s_{0,1}\rangle &= \frac{\alpha|0\rangle + \beta(\cos\theta \mp \sin\theta)|1\rangle}{\sqrt{2}} \\ &\approx \frac{\alpha|0\rangle + \beta(1 \mp \theta - \frac{\theta^2}{2})|1\rangle}{\sqrt{2}}. \end{aligned} \quad (2.1)$$

In the last step, we used that  $\theta \ll 1$ . We retained the second-order term for  $\theta$  because this is a first-order contribution in  $dt$ . Weak measurement is performed over the system

---

<sup>†</sup>For example,  $\text{CNOT}|0, \phi\rangle = |0, \phi\rangle$  and  $\text{CNOT}|1, \phi\rangle = |1, \sigma_1\phi\rangle$

when we do a projective measurement over the ancilla. The latter can be done by the subsystem projectors:

$$\Pi_n = \hat{1} \otimes |n\rangle\langle n|,$$

where  $n = \{0, 1\}$ . Therefore, after measuring the ancillary qubit, the total system will change by

$$|\Psi'\rangle \rightarrow \Pi_n |\Psi'\rangle / \sqrt{p_n},$$

where  $p_n = \langle \Psi' | \Pi_n | \Psi' \rangle$  is the probability that the ancilla is in the state  $|n\rangle$ . Hence, the total system change will be

$$|\Psi'\rangle \rightarrow \frac{\Pi_n |\Psi'\rangle}{\sqrt{\langle \Psi' | \Pi_n | \Psi' \rangle}} = |\psi'_n\rangle \otimes |n\rangle,$$

where  $|\psi'_n\rangle = |s_n\rangle / \sqrt{\langle s_n | s_n \rangle}$  is the system state after the measurement over the ancilla has been performed. Once we know the measurement result, no entanglement remains between the subsystems. Therefore, the ancilla can be discarded by tracing it out. We can from now on speak of an effective *weak measurement* over the system, with its state changing according to

$$|\psi\rangle \rightarrow |\psi'_n\rangle = |s_n\rangle / \sqrt{p_n},$$

after a weak measurement, with probability  $p_n = \langle s_n | s_n \rangle$ , where  $n = \{0, 1\}$  keep track of the ancilla measurement result. The states  $|s_n\rangle$  are given by equation (2.1). To be more specific, the probability to (weakly) measure  $|\psi'_0\rangle$  is

$$p_0 = \frac{|\alpha|^2 + |\beta|^2 \left(1 - \theta - \frac{\theta^2}{2}\right)^2}{2} \approx \frac{1}{2} - \theta|\beta|^2, \quad (2.2)$$

where

$$\begin{aligned} |\psi'_0\rangle &= (1 - 2\theta|\beta|^2)^{-1/2} \left[ \alpha |0\rangle + \beta \left(1 - \theta - \frac{\theta^2}{2}\right) |1\rangle \right], \\ &\approx \left(1 + \theta|\beta|^2 + \frac{3}{2}\theta^2|\beta|^4\right) \left[ \alpha |0\rangle + \beta \left(1 - \theta - \frac{\theta^2}{2}\right) |1\rangle \right]. \end{aligned}$$

In the last step, we expanded the denominator up to  $\mathcal{O}(\theta^2)$  (included). After multiplication of the factors and further simplifications, we finally obtain:

$$|\psi'_0\rangle = \alpha \left(1 + \theta|\beta|^2 + \frac{3}{2}\theta^2|\beta|^4\right) |0\rangle + \beta \left(1 - |\alpha|^2\theta - |\beta|^2\theta^2 - \frac{\theta^2}{2} + 3|\beta|^4\frac{\theta^2}{2}\right) |1\rangle. \quad (2.3)$$

For  $p_1$  and  $|\psi'_1\rangle$ , it suffices to change the sign  $\theta \rightarrow -\theta$  in Eqs. (2.2) and (2.3), so that

$$p_1 \approx \frac{1}{2} + \theta|\beta|^2, \quad (2.4)$$

and

$$|\psi'_1\rangle = \alpha \left( 1 - \theta|\beta|^2 + \frac{3}{2}\theta^2|\beta^2| \right) |0\rangle + \beta \left( 1 + |\alpha|^2\theta - |\beta|^2\theta^2 - \frac{\theta^2}{2} + 3|\beta|^4\frac{\theta^2}{2} \right) |1\rangle. \quad (2.5)$$

Defining the state differential as  $d|\psi\rangle \equiv |\psi'\rangle - |\psi\rangle$ , the two measurement possibilities  $|\psi'_0\rangle$  and  $|\psi'_1\rangle$  can be cast into a single equation:

$$d|\psi\rangle = \alpha \left( \pm\theta|\beta|^2 + \frac{3}{2}\theta^2|\beta|^4 \right) |0\rangle + \beta \left( \mp|\alpha|^2\theta - |\beta|^2\theta^2 - \frac{\theta^2}{2} + 3|\beta|^4\frac{\theta^2}{2} \right) |1\rangle, \quad (2.6)$$

with probability

$$p = \frac{1}{2} \mp \theta|\beta|^2, \quad (2.7)$$

for each outcome, respectively. To deduce the Stochastic Schrödinger Equation (SSE) in time, we have to express  $d|\psi\rangle$  in terms of the Lindblad operator  $L$  [35], which here is given by:

$$L = \frac{\theta}{\sqrt{\eta dt}} |1\rangle\langle 1|, \quad (2.8)$$

where  $\eta$  is the measurement rate and  $dt$  is the time interval between any two measurements. This Lindblad operator characterizes how the system interacts with the ancilla. Its form depends on the measurement protocol chosen. The somewhat odd scaling  $\theta/\sqrt{\eta dt}$  reflects the fact that  $\theta \propto \sqrt{\eta dt}$ . The constant of proportionality can be set to 1 without loss of generality. But for now, we will keep it explicitly in Eq. (2.8) to keep track of terms that will appear. To introduce the Lindblad operator into Eq. (2.6), the following relations are useful:

$$\begin{aligned} |\beta|^2 &= \frac{\sqrt{\eta dt}}{\theta} \langle L \rangle = \frac{\sqrt{\eta dt}}{\theta} \langle L^\dagger \rangle, \\ |\beta|^4 &= \frac{\eta dt}{\theta^2} \langle L \rangle, \\ \beta |1\rangle &= \frac{\sqrt{\eta dt}}{\theta} L |\psi\rangle = \frac{\eta dt}{\theta^2} L^\dagger L |\psi\rangle = \frac{\eta dt}{\theta^2} L L^\dagger |\psi\rangle. \end{aligned}$$

Introducing them into Eq. (2.6), we get:

$$d|\psi\rangle = \frac{1}{2} \left( 3 \langle \hat{L} \rangle^2 - 2 \langle \hat{L}^\dagger \rangle \hat{L} - \hat{L}^\dagger \hat{L} \right) |\psi\rangle \eta dt + (\hat{L} - \langle \hat{L} \rangle) |\psi\rangle dZ \quad (2.9)$$

The noise  $dZ = \pm\sqrt{\eta dt}$  is a discrete random number. Each outcome has, respectively, a probability  $p = 1/2 \pm \theta|\beta|^2 = 1/2 \pm \sqrt{\eta dt} \langle L^\dagger \rangle$  to occur. Consequently, the mean value of  $dZ$  is equal to

$$\overline{dZ} = \left(\frac{1}{2} + \sqrt{\eta dt} \langle L^\dagger \rangle\right) (+\sqrt{\eta dt}) + \left(\frac{1}{2} - \sqrt{\eta dt} \langle L^\dagger \rangle\right) (-\sqrt{\eta dt}) = 2\eta dt \langle \hat{L}^\dagger \rangle.$$

It is more convenient, however, to work with zero average noise. For this reason, we will work with the white noise  $dW$ , where  $dW = dZ - 2\eta dt \langle L^\dagger \rangle$ , and  $dW^2 = \eta dt + \mathcal{O}((\eta dt)^{3/2})$ . Substituting  $dZ = dW + 2\eta dt \langle L^\dagger \rangle$  into Eq. (2.9), the SSE can finally be expressed in the nonunitary diffusive form [35]:

$$d|\psi\rangle = |\psi_{t+dt}\rangle - |\psi_t\rangle = \left\{ -\frac{1}{2}(L - \langle L \rangle)^2 \eta dt + (L - \langle L \rangle) dW \right\} |\psi_t\rangle. \quad (2.10)$$

We can now get rid of the odd scaling  $\sim \theta/\sqrt{\eta dt}$  of  $L$  by fixing  $\theta = \sqrt{\eta dt}$ . This constraint is consistent with continuous monitoring, since  $\theta \rightarrow 0$  as  $dt \rightarrow 0$ . Therefore,

$$L = |1\rangle\langle 1|.$$

Eq. (2.10) defines a quantum trajectory for  $|\psi_t\rangle$ . This equation is non-linear, because of the presence of the term  $\langle L \rangle = \langle \psi | L | \psi \rangle$ . The contribution  $\propto \eta dt$  in the SSE will lead to different trajectories only for different initial states  $|\psi_0\rangle = \alpha |0\rangle + \beta |1\rangle$ . Consequently, this term is deterministic. On the other hand, due to the probabilistic nature of the measurement over the ancilla, we get a noisy factor in the SSE that is proportional to  $dW = \pm\sqrt{\eta dt} + \mathcal{O}((\eta dt)^{3/2})$ , where each outcome has a probability  $p = 1/2 \pm \mathcal{O}((\eta dt)^{1/2})$ . This is the stochastic contribution of the SSE. In the continuous limit  $dt \rightarrow 0$ , we can safely state that  $dW = \pm\sqrt{\eta dt}$  with equal probability for the two outcomes. Setting the initial condition, each stream of random numbers  $dW$  will define a different quantum trajectory for  $|\psi_t\rangle$ .

It is worth mentioning that we ignored contributions from kinetic energy and external potential encoded in the Hamiltonian  $H$ . We will restrict to analyze only the changes induced by measurement in the state  $|\psi\rangle$ . To introduce such effects, it suffices to add  $-i/\hbar H |\psi_t\rangle dt$  on the right-hand side of the Eq. (2.10).

Although Eq. (2.10) is perfectly good for describing the nonunitary diffusion of initial pure states, It cannot describe situations where the initial state is mixed. To deal with the latter, we need to know how a density matrix evolves under continuous monitoring.

This brings us to the Stochastic Master Equation (SME) for non-unitary diffusion.

## 2.2 Stochastic Master Equation (SME)

To start with a fully mixed state, we need to know the stochastic differential equation that describes the density matrix  $\rho = \rho_t$  evolution at any time  $t$ . This equation is commonly named the *Stochastic Master equation* (SME). For a pure state  $|\psi_t\rangle$ , the density matrix is simply  $\rho_t = |\psi_t\rangle\langle\psi_t|$ . Hence

$$\rho_{t+dt} = \rho_t + d\rho = (|\psi_t\rangle + d|\psi\rangle)(\langle\psi_t| + d\langle\psi|),$$

where  $d|\psi\rangle = |\psi_{t+dt}\rangle - |\psi_t\rangle$  and  $d\rho = \rho_{t+dt} - \rho_t$ . Substituting Eq. (2.10) into the equation above, the SME can be written in the following concise form:

$$d\rho = \rho_{t+dt} - \rho_t = -\frac{1}{2}[L, [L, \rho_t]]\eta dt + (\rho_t L + L\rho_t - 2\langle L \rangle \rho_t)dW, \quad (2.11)$$

where  $dW = \pm\sqrt{\eta dt}$  with equal probability,  $L = |1\rangle\langle 1|$  and  $\langle L \rangle = \text{tr}(\rho_t L)$ . Although Eq. (2.11) was derived for the case of a pure state, it remains valid even when the system is in a mixed state. This can be shown by employing *Positive Operator Valued Measurements* (POVM) operators instead of the approach we used in section 2.1, where we monitored the ancilla qubits. The outline of how to use POVMs to arrive at equation (2.11) is given in the appendix A.

To incorporate a unitary evolution governed by a Hamiltonian  $H$ , the Von-Neumann-Liouville term [39, 36] must be included into Eq. (2.11). The result is:

$$d\rho = \rho_{t+dt} - \rho_t = -\frac{i}{\hbar}[H, \rho_t]\eta dt - \frac{1}{2}[L, [L, \rho_t]]dt + (\rho_t L + L\rho_t - 2\langle L \rangle \rho_t)dW.$$

Eq. (2.11) describes the state  $\rho_t$  of the system conditioned on the measurement outcome of the ancilla. If the ancilla is not measured, we should average the evolution over the possible results. Defining  $\sigma \equiv \bar{\rho}$ , where the overline denotes the average over-measurement outcomes, the evolution of  $\sigma_t$  is given by the following Lindblad equation:

$$d\sigma = \sigma_{t+dt} - \sigma_t = -\frac{1}{2}[L, [L, \sigma_t]]\eta dt, \quad (2.12)$$

which describes the evolution of an open quantum system [34, 40]. Starting with a pure state  $\sigma_0 = |\psi\rangle\langle\psi|$ , Eq. (2.12) will drive the system to a mixed state  $\sigma = \hat{1}/2$ .

The reason is the unitary interaction with the ancilla at each time interval  $dt$ , which irreversibly scrambles the initial information. Therefore, the deterministic part of the SME introduces decoherence into the system by canceling off-diagonal terms. This is the opposite of equation (2.11), which, starting in a mixed state, time evolution drives the system to a pure state by successive weak measurements over it.

The continuous monitoring purification can be simulated by iterating equation (2.11) with a finite step  $\Delta t$  and using a (pseudo) random number generator to simulate the noise. As our focus lies in purifying a mixed (diagonal) state, the time evolution of the density matrix can be encapsulated by one parameter, delineated by a stochastic differential equation, also known as a Langevin equation.

## 2.3 Langevin equation of non-unitary diffusion quantum trajectories

When continuously measuring a qubit, its state will evolve according to Eq. (2.11). Therefore, starting in a mixed state  $\rho_0 = \hat{1}/2$ , off-diagonal terms will not be introduced by monitoring. As a result, the density matrix  $\rho_t$  can be expressed by a single dynamic variable  $q = q(t)$  without loss of generality. We will represent the density matrix by

$$\rho_t = \rho(q) = \frac{1+q}{2} |0\rangle\langle 0| + \frac{1-q}{2} |1\rangle\langle 1| = \frac{1+q\sigma_3}{2}, \quad (2.13)$$

where  $\sigma_3 = \text{diag}(1, -1)$  and  $q(0) = 0$ . The pure states  $\rho = |0\rangle\langle 0|$  and  $\rho = |1\rangle\langle 1|$  are mapped into  $q = 1$  and  $q = -1$ , respectively. Time evolution for the parameter  $q$  is defined by substituting Eq. (2.13) into Eq. (2.11), resulting in the following stochastic differential equation for  $q$ :

$$dq = (1 - q^2)dW, \quad (2.14)$$

where  $dq = q(t + dt) - q(t)$  and  $dW = \pm\sqrt{\eta dt}$  with equal probability. When  $q = \pm 1$ , the increment  $dq$  is set to zero. So  $q$  is restricted in the interval  $-1 \leq q \leq 1$  by Eq. (2.14). The increment  $dt$  is interpreted as an infinitesimal time interval for the continuous time  $t$ . In this limit, the discrete noise  $dW$  can be, at any time, substituted by a Gaussian noise where  $\langle dW(t) \rangle = 0$  and  $\langle dW(t)dW(t') \rangle = \eta dt^2 \delta(t - t')$ , where the average  $\langle \dots \rangle$  is calculated over the noise distribution. Eq. (2.14) can also be expressed in the canonical

Langevin's equation form (see appendix [B](#) for more details on Langevin's equation):

$$\frac{dq}{dt} \stackrel{\alpha=0}{=} g(q)W(t), \quad (2.15)$$

where  $g(q) = 1 - q^2$  is the noise amplitude and  $W(t)$  is a gaussian white noise with  $\langle W(t)W(t') \rangle = \eta\delta(t - t')$ . Since this equation has a multiplicative noise  $g(q)W$ , a proper time regularization has to be defined. This is specified by the index  $\alpha = 0$  above the equality, signifying that Eq. [\(2.15\)](#) is discretized in time in the Itô sense (see appendix [B.1](#) for more details on time discretization issues). We define the discrete-time by dividing the time interval of size  $t$  into  $N$  equal parts of size  $\Delta t = t/N$ . Consequently, time is now labeled by an integer index  $n$ , becoming  $t_n = n\Delta t$ , where  $n = 0, 1, \dots, N$ , and position is defined by  $q_n \equiv q(t_n)$ . With that being stated, the exact meaning of Eq. [\(2.15\)](#) is:

$$\frac{\Delta q}{\Delta t} = g(q_n)W_n, \quad (2.16)$$

where  $\Delta q = q_{n+1} - q_n$  and  $\langle W_n W_{n'} \rangle = \eta\Delta t^{-1}\delta_{n,n'}$ <sup>‡</sup>. Or, equivalently

$$\Delta q = g(q_n)\Delta W_n, \quad (2.17)$$

where  $\langle \Delta W_n \rangle = 0$ ,  $\langle \Delta W_n \Delta W_{n'} \rangle = \eta\Delta t\delta_{n,n'}$  and  $g(q_n) = 1 - q_n^2$ . Using a pseudo number generator to compute the Gaussian noise  $\Delta W_n$ , the continuous measurement quantum trajectories can be numerically calculated by iterating equation [\(2.17\)](#).

---

<sup>‡</sup>We used

$$\delta(t_n - t_{n'}) = \lim_{\Delta t \rightarrow 0} \Delta t^{-1}\delta_{n,n'}.$$



# Chapter 3

## Quantum trajectories numerical simulation

Once in the hand of the Stochastic differential equation that describes the state evolution in time (Eq. (2.17)), we can numerically simulate it. One can achieve this by repeatedly running it on a computer, generating a random number at each iteration, and substituting it into Eq. (2.17) to determine the subsequent data point. By this procedure, we can generate a set of points  $\{q_0, q_1, \dots\}$  that, when connected, will represent the non-unitary quantum trajectory formally deduced in the previous chapter. Likewise, once we have the set of points from a particular quantum trajectory, we also have access to the time evolution of any observable of the form  $\hat{\mathcal{O}}(\rho)$ , as the latter can be expressed as a simple function  $\mathcal{O}(q)$  by mean of Eq. (2.13). Since we are interested in the purification of the state, we will calculate the trajectories of the purity, the Von-Neumann entropy, and the information gained when continuously monitoring the system, as their probability distributions.

### 3.1 Method

A quantum trajectory is calculated by iterating the equation

$$\Delta q = q_{n+1} - q_n = g(q_n)\Delta W_n, \quad (3.1)$$

for each time step of size  $\Delta t$ , in the same spirit as Euler's method [41] for numerically integrating ordinary differential equations. However, unlike the latter, Eq. (3.1) has a

noisy term  $\Delta W_n \equiv W(t_n)\Delta t$  that has to be computed at each step by a random number generator. The extension of the Euler method incorporating a random term is called the Euler-Maruyama method [27], and it will be employed for computing the quantum trajectories from now on. Since  $\Delta W_n$  is Gaussian white noise such that  $\langle \Delta W_n \Delta W_{n'} \rangle = \eta \Delta t \delta_{n,n'}$ , its probability distribution at time  $t_n = n\Delta t$  will be:

$$P_{\text{noise}}(\Delta W_n) = \frac{1}{\sqrt{2\pi\eta\Delta t}} e^{-\frac{(\Delta W_n)^2}{2\eta\Delta t}}. \quad (3.2)$$

A Gaussian distributed random number  $\Delta W_n$  is easily generated by a computer using pseudorandom numbers (see [41] for technical details about how to do it). Symbolically, we will denote  $\Delta W_n \sim \mathcal{N}(0, \eta\Delta t)$  as a random number generated by the Normal distribution with an average equal to zero and variance  $\sigma^2 = \eta\Delta t$ . To generate a quantum trajectory, we have to calculate a stream of  $N$  random numbers  $\{\Delta W_0, \Delta W_1, \dots, \Delta W_{N-1}\} \equiv \{\Delta W_n\}$ , which we will call the *noise realization* for  $\Delta W_n$ . With it, we can generate a quantum trajectory  $\{q_0, \dots, q_N\} \equiv \{q_n\}$  by iterating  $N$  times the recurrence relation:

$$q_{n+1} = q_n + g(q_n)\Delta W_n, \quad (3.3)$$

where  $q_0 = q(t=0)$  is fixed for all trajectories. Once obtained  $\{q_n\}$ , we can trivially obtain the trajectories of an observable  $\hat{O}(\rho)$  by computing  $\{\mathcal{O}(q_0), \dots, \mathcal{O}(q_N)\} \equiv \{\mathcal{O}_n\}$ . Naturally, because each noise realization will be different from one another, every time we run the algorithm for the same initial condition, a different trajectory is also obtained.

For all the simulations obtained in this chapter, we used  $q_0 = 0$ ,  $\eta = 1$ , and  $\Delta t = 0.001$ . The time interval has to be small because the Central limit theorem is only valid for all  $t$  in the limit  $\Delta t \rightarrow 0$ . For example, if one considers  $\Delta t = 0.01$ , small discrepancies between simulation and theoretical results (built in a subsequent chapter upon Gaussian noise) will appear at small times for the probability distribution. At each step, noise is calculated using  $\Delta W_n \sim \mathcal{N}(0, \eta\Delta t)$  from a pseudo-random number generator of a computer program.

---

\*More generally, if  $X$  is a random variable such that  $X \sim \mathcal{N}(\mu, \sigma^2)$ , then

$$P(X = x) = \frac{1}{\sqrt{2\pi\sigma^2}} \exp\left(-\frac{(x - \mu)^2}{2\sigma^2}\right)$$

where  $P(X = x)$  is the density probability distribution of  $X$ .

## 3.2 Non-unitary diffusion quantum trajectories

Using the method described in the previous section, numerical integration of the equation:

$$\Delta q_n = g(q_n)\Delta W_n,$$

for five different replicas of the qubit, yield the following trajectories:

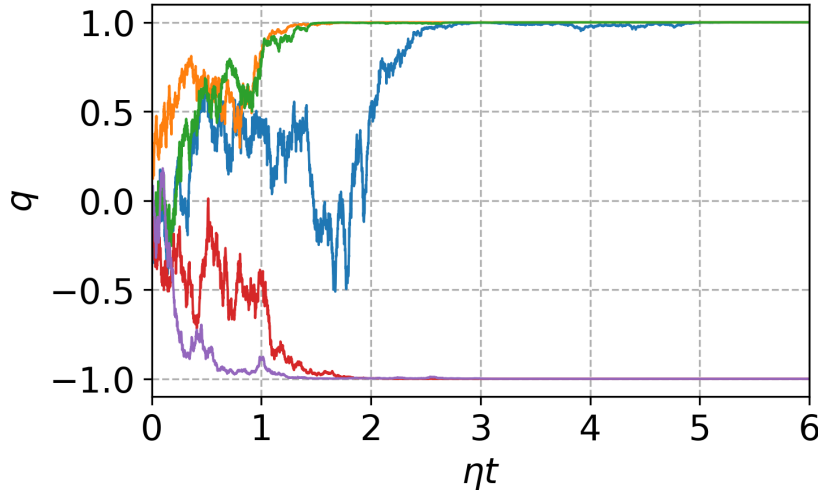


**Figure 3.1:** Five noise realization of Eq. (3.3), calculated with  $q_0 = 0$ ,  $\eta\Delta t = 0.001$  and  $\Delta W_n \sim \mathcal{N}(0, \sigma^2 = \eta\Delta t)$

From Fig. 3.1, we see that all trajectories tend to  $q \rightarrow \pm 1$ , and remain fixed there once this value is attained. This physically translates as the system being purified into states  $\rho = |0\rangle\langle 0|$  or  $\rho = |1\rangle\langle 1|$ , respectively.

Despite the stochastic nature of a single trajectory, many replicas of them yields a very precise probability distribution  $P_q(q, t)$ , defined in the interval  $-1 \leq q \leq 1$  and  $t \geq 0$ , with  $P_q(q, 0) = \delta(q)$  as the initial condition. At this stage, we do not know the precise analytical expression for  $P_q(q, t)$ . Nevertheless, the simulation can accurately calculate a histogram for the position  $q(t)$  of the trajectories at a specific time  $t$ . Below are histograms at times  $\eta t = 0.1, 0.5, 2$ , calculated with  $N = 100,000$  trajectories.

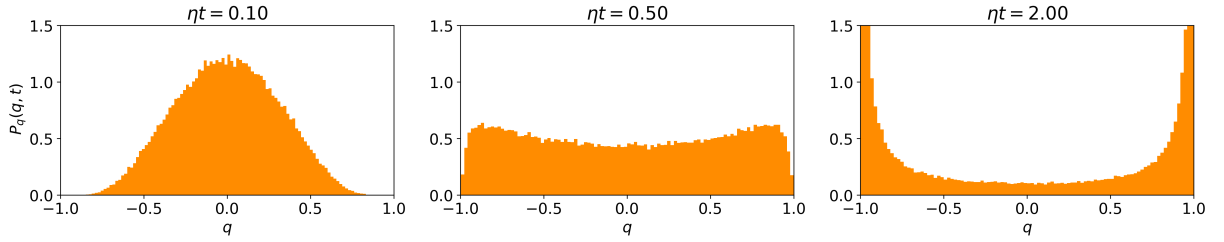


**Figure 3.2:** Probability distribution  $P_q(q, t)$  at times  $\eta t = 0.1, 0.5$  and  $2.0$ . Calculations were performed with 100,000 samples of Eq. (3.3), with  $\eta\Delta t = 0.001$ .

We see from Fig. 3.2 that, as time evolves, the probability distribution tends to be sharpened and peaked at the edges  $q = \pm 1$ . This is indeed the expected behavior, since all trajectories will end up being purified at large times.

With the replicas of the trajectories, we can calculate any moment  $\langle q^k \rangle$  of  $q$ , where  $k$  is a natural number. By defining the  $i$ -th trajectory calculated with Eq. (3.3) by  $q_i(t)$ , the  $k$ -th moment evaluated at time  $t$  will be:

$$\langle q^k \rangle = \int_{-1}^1 dq P_q(q, t) q^k \approx \frac{1}{N} \sum_{i=1}^N q_i(t)^k, \quad (3.4)$$

where  $N$  is the number of the system copies in this context (not to confuse with  $N = t/\Delta t$  used in the previous section, which was equal to the number of time slices). Equality between the integral and the sum occurs in the limit where  $N \rightarrow \infty$ . In this limit, statistical fluctuations of the averages, typically of order  $\sim 1/\sqrt{N}$ , go to zero. Particularly, with Eq. (3.4) we calculated the expected value  $E[q] = \langle q \rangle$  and the variance  $\text{Var}[q] = \langle q^2 \rangle - \langle q \rangle^2$  for  $N = 100,000$  trajectories. These two quantities provide important information about the average behavior of  $P_q(q, t)$  and its deviations, respectively. The result can be seen below, in Fig. 3.3.

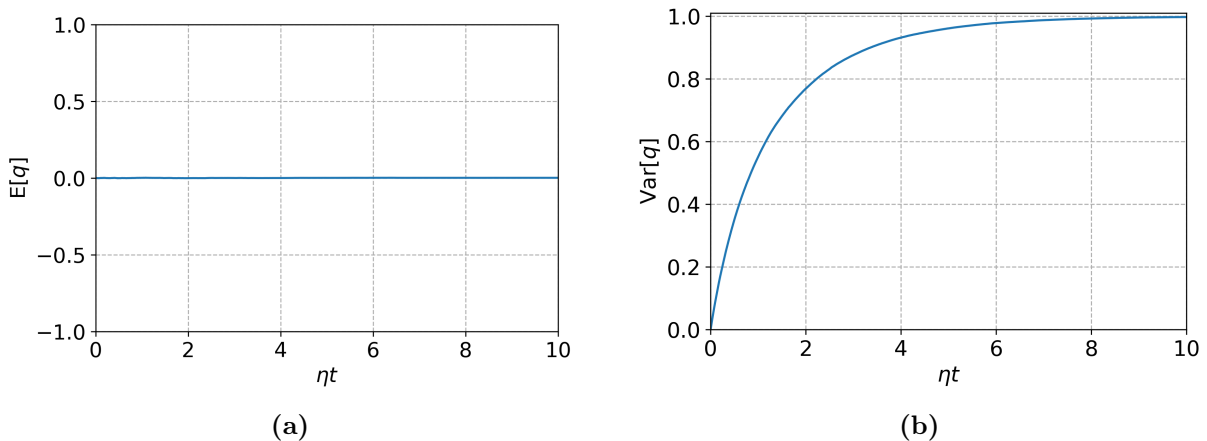


**Figure 3.3:** Expected value (left) and variance (right) of the distribution  $P_q(q, t)$ . Calculations were performed with  $N = 100,000$  samples of Eq. (3.4). We used  $\eta\Delta t = 0.001$  for the time grid.

For  $N = 100,000$  samples, fluctuations will be of order  $\sim 10^{-3}$ , hence the curves in Fig. 3.3 are precise up to the second digit. In figure 3.3a we have numerical evidence that  $\langle q \rangle = 0$  for all  $t$ , a consequence of the even parity of  $P_q(q, t)$ . This physically means that half of the qubits will be purified into state  $|0\rangle$  and half into state  $|1\rangle$ . The variance calculated in Fig. 3.3b tends to one as  $\eta t \rightarrow \infty$ , which is consistent with  $q \rightarrow \pm 1$  in this limit.

### 3.3 Observables of interest

From the statistical behavior of the trajectories, we can similarly study the behavior of an observable  $\hat{\mathcal{O}}(\rho)$  which is a function of the qubit state at a given time. By observable, we mean a quantity that can in principle be measured, directly or indirectly, and which gives relevant information about the system [39, 42]. In our scenario, we are particularly interested in quantifying how close is the qubit to a pure state, which is assessed by the purity. Additionally, we aim to measure the amount of information extracted from the system, which is quantified by the entropy and information gain. This section is organized in a similar way to the previous: we show the stochastic trajectories  $\{\mathcal{O}_n\}$  for each observable mentioned, as its probability distributions  $P_{\mathcal{O}}(\mathcal{O}, t)$ , expected values  $E[\mathcal{O}] = \langle \mathcal{O} \rangle$  and variances  $\text{Var}[\mathcal{O}] = \langle \mathcal{O}^2 \rangle - \langle \mathcal{O} \rangle^2$ . As before, once we know how to obtain replicas for the trajectories  $\{\mathcal{O}_n\}$ , we can calculate any moment  $\langle \mathcal{O}^k \rangle$  of the observable by:

$$\langle \mathcal{O}^k \rangle = \int d\mathcal{O} P_{\mathcal{O}}(\mathcal{O}, t) \mathcal{O}^k \approx \frac{1}{N} \sum_{i=1}^N \mathcal{O}(q_i(t))^k, \quad (3.5)$$

with equality between the sum and the integral occurring in the limit  $N \rightarrow \infty$ . The integral is performed over the observable domain.

### 3.3.1 Purity

To quantify how close a system is to a pure state, we will use the purity, defined for a system in the state  $\rho$  by:

$$\tau(\rho) = \text{tr } \rho^2. \quad (3.6)$$

For a qubit in a mixed state, it is easily shown that  $\tau = \frac{1}{2}$ . While once in a pure state, then  $\tau = \text{tr } \rho^2 = \text{tr } \rho = 1$ . Hence, by continuously measuring a mixed state, the purity will change from  $\frac{1}{2} \leq \tau \leq 1$ , where  $\tau = 1$  indicates that a pure state has been reached. Substituting Eq. (2.13) into Eq. (3.6), the purity is defined as a function of  $q$  by:

$$\tau(q) = \frac{1 + q^2}{2}, \quad (3.7)$$

where  $q = q(t)$  evolves according to (2.17) in discrete time. As a result, the trajectories  $\{\tau_n\}$  are easily determined from  $\{q_n\}$ . Below are the correspondent purity trajectories for the five noise realizations depicted in Fig. 3.1:

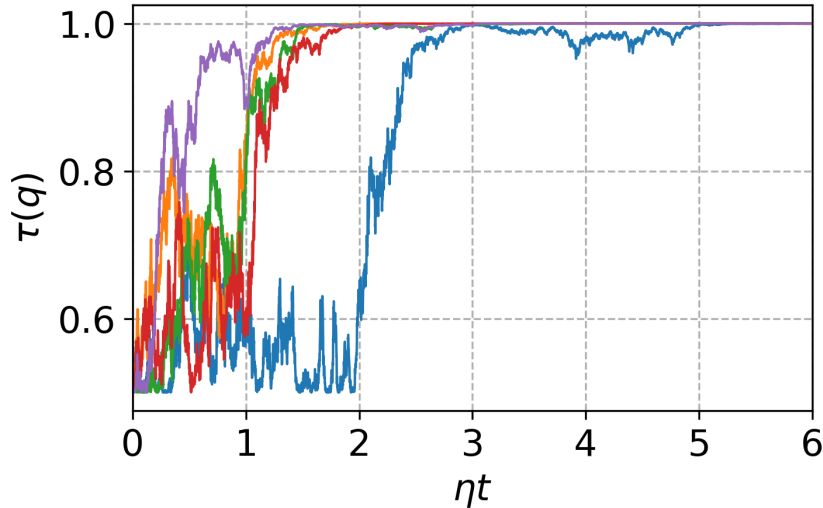


**Figure 3.4:** Purity  $\tau(q)$  for the trajectories depicted in Fig. 3.1

All purity stochastic trajectories start at  $\tau = \frac{1}{2}$  and, in the long run, will end purified with  $\tau = 1$ , as is readily seen from Fig. 3.4.

The probability distribution of the values  $\tau$  over time is defined by  $P_\tau(\tau, t)$ , with domain  $\frac{1}{2} \leq \tau \leq 1$  and  $t \geq 0$ . Initial condition  $P_\tau(\tau, 0) = 2\delta(\tau - \frac{1}{2})$  is automatically

satisfied by setting  $q_0 = 0$  for all quantum trajectories. For  $t > 0$ , we can calculate  $P_\tau(\tau, t)$  by generating an ensemble of trajectories for  $\{\tau_n\}$  and plot the various results at a fixed time in the form of a histogram, as we did for  $P_q(q, t)$  in Fig. 3.2. Histograms calculated from  $N = 100,000$  trajectories at three different times are depicted in Fig. 3.5 below:

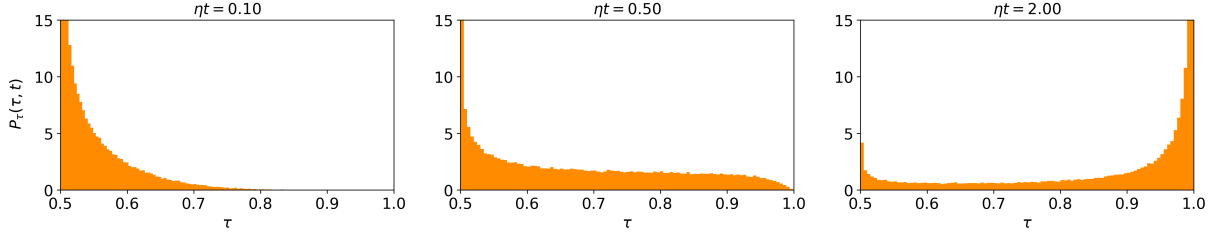


**Figure 3.5:** Probability distribution  $P_\tau(\tau, t)$  at times  $\eta t = 0.1, 0.5$  and  $2.0$ . Calculations were performed with 100,000 samples of Eq. (3.7), using  $\eta\Delta t = 0.001$  in Eq. 3.3

From Fig. 3.5, we observe that the purity distribution changes from  $\tau = \frac{1}{2}$  to  $\tau = 1$  as time evolves, with via a two-peak structure at intermediate times.

Substituting  $\mathcal{O} = \tau$  into Eq. (3.5), we obtain the expected value  $E[\tau] = \frac{1 + \langle q^2 \rangle}{2}$  and the variance  $\text{Var}[\tau] = \frac{\langle q^4 \rangle - \langle q^2 \rangle^2}{4}$  for the purity. The results are depicted below in Fig. 3.6

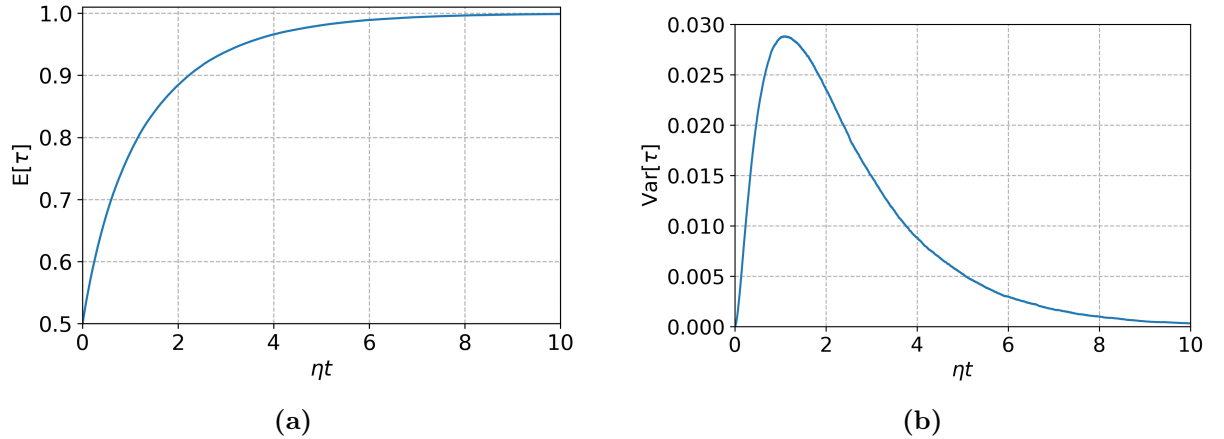


**Figure 3.6:** Expected value (left) and variance (right) of the distribution  $P_\tau(\tau, t)$ . Calculations were performed with 100,000 samples generated by Eq. (3.4). We used  $\eta\Delta t = 0.001$  for the time grid.

Within  $0 \leq \eta t < \infty$ , the expected value for  $\tau$  evolves from  $0 \leq \tau \leq 1$ , with fluctuations equal to zero in the extremes, attaining a maximum value at  $\eta t \approx 1.1$ .

### 3.3.2 Von-Neumann entropy and information gain

The Von-Neumann entropy of a qubit in state  $\rho$  is defined as:

$$S(\rho) = -\text{tr}(\rho \log \rho), \quad (3.8)$$

where  $\log 2 = 1$  and  $0 \log 0 \equiv 0$ . This function is useful in quantifying the amount of uncertainty we have about the qubit state. More precisely, maximum uncertainty is attained by the mixed state  $\rho_{\text{mixed}} = \hat{1}/2$ . Physically this state can represent an unpolarized photon from a malfunctioning laser, for example, where states  $|0\rangle$  and  $|1\rangle$  denote the horizontal and vertical polarization of the photon, respectively. In this case, it is easy to show that  $S(\rho_{\text{mixed}}) = 1$ , which implies in a total ignorance of the photon polarization before measurement (unpolarized pulse of light). For pure states, generated by the ideal laser, for example, we can always choose a basis where  $\rho_{\text{pure}} = \text{diag}(1, 0)$  by simply rotating the polarizer<sup>†</sup> in the direction that maximizes the signal. In this representation, it is trivial to show that  $S(\rho_{\text{pure}}) = 0$ , meaning we have complete information about the photon polarization state from the laser [43].

From the observer's point of view, however, it makes more sense to speak of the information gained rather than the uncertainty of the system state. Assuming that no loss of information occurs from the measurement process, we quantify the gain of information as the reduction in uncertainty about the system due to measurement. Thus, if  $I(\rho)$  is the information gained, then:

$$I(\rho) = -\Delta S = -(S(\rho) - S(\rho_0)).$$

Where  $\rho_0$  is the state of the system before measurement starts. Since in our case  $\rho_0 = \rho_{\text{mixed}}$ , then

$$I(\rho) = 1 - S(\rho). \quad (3.9)$$

If no measurement has occurred, then  $I = 0$ , hence no information about the system has been extracted. Conversely, if a pure state has been attained, then  $I = 1$ , that is, all information has been extracted from the qubit. In between these extreme cases, we have partial information about the state of the system.

When we continuously measure a single qubit in a mixed state, the values for the

---

<sup>†</sup>Polarizer is an experimental apparatus that measure the intensity of light at a certain direction. The light signal is converted into an amplified electronic signal that is displayed into a digital screen.



entropy will evolve in a stochastic manner from  $S = 1$  to  $S = 0$  for  $0 \leq t < \infty$ . A specific noise realization for the entropy is defined by substituting Eq. (2.13) into Eq. (3.8), resulting in:

$$S(q) = -\frac{1+q}{2} \log\left(\frac{1+q}{2}\right) - \frac{1-q}{2} \log\left(\frac{1-q}{2}\right), \quad (3.10)$$

where a trajectory  $\{q_n\}$  for  $q$  is generated iterating equation (3.3). Likewise,

$$I(q) = 1 - S(q), \quad (3.11)$$

where the information increases from  $I = 0$  to  $I = 1$  as  $q$  randomly drifts from  $q = 0$  to  $q = \pm 1$ . The trajectories for the entropy for the five replicas state evolution depicted in Fig. 3.1 is depicted below:

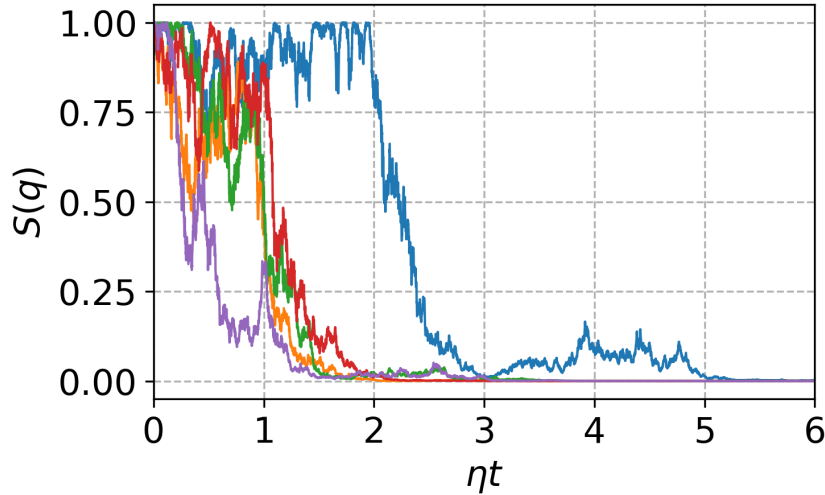


**Figure 3.7:** Purity  $S(q)$  for the trajectories depicted in Fig. 3.1

All stochastic curves start in  $S = 1$  and drift to  $S = 0$  as purification grows continuously. The stochastic curves for the information are not shown here, since they have the same behavior for the trajectories in Fig. 3.7, but only reflected over the line  $S = 0.5$ . Similarly to the purity, we can calculate probability distributions for  $P_S(S, t)$  and  $P_I(I, t)$  by simulating ensembles of trajectories for  $\{S_n\}$  and  $\{I_n\}$ , respectively. Distributions  $P_I$  and  $P_S$  are trivially related to each other by  $P_S(S, t) = P_I(1 - S, t)$ . Below we plot both probability distributions calculated from an ensemble of  $N = 100,000$  trajectories generated with Eq. (3.3):

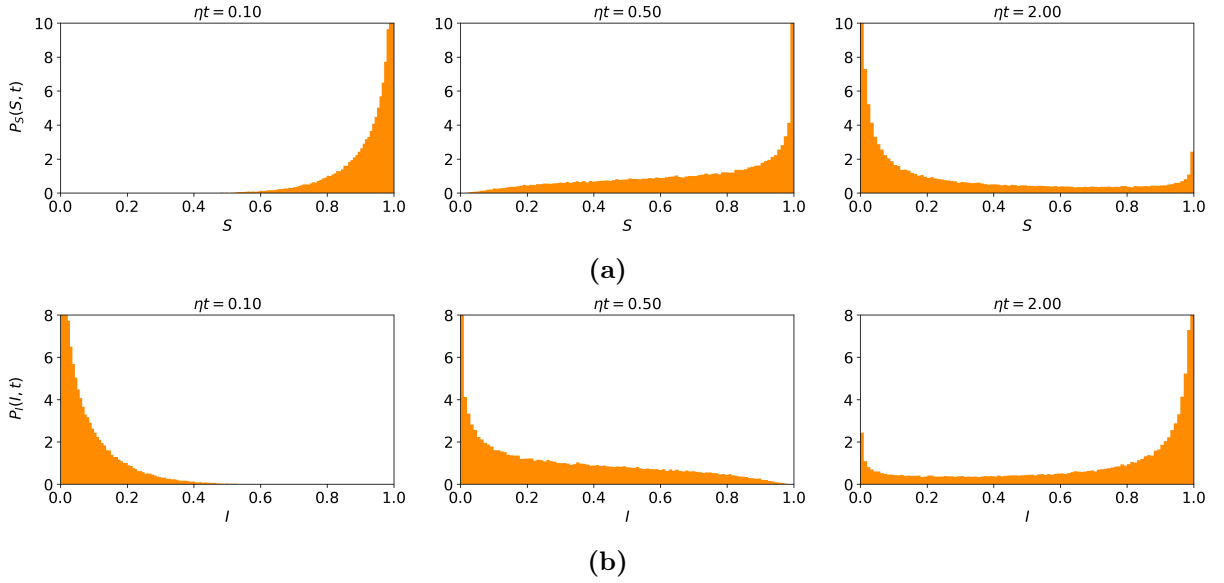


**Figure 3.8:** Probability distributions  $P_S(S, t)$  (3.8a) and  $P_I(I, t)$  (3.8b) calculated with  $N = 100,000$  samples of equation (3.3). we used  $\eta\Delta t = 0.001$  for the time grid.

In Figs. 3.8 we see that for short times, as in  $\eta t = 0.01$ , the entropy (information gain) is distributed next to  $S = 1$  ( $I = 0$ ). As we measure the system, intermediate values of the entropy (information gain) contribute more and more. Finally, a second peak appears at  $S = 0$  ( $I = 1$ ), as is manifest at  $\eta t = 2.0$ , but without the occurrence of distinct peak at intermediate values. Therefore, information is transported more abruptly than one would intuitively expect from a definite peak continuously drifting from  $I = 0$  to  $I = 1$ .

Finally, expected values  $E[S]$  and  $E[I]$  and variance  $\text{Var}[S](= \text{Var}[I])$ , calculated substituting  $\mathcal{O} = S$  and  $\mathcal{O} = I$  into Eq. (3.5), can be seen in the Fig. 3.9 below:

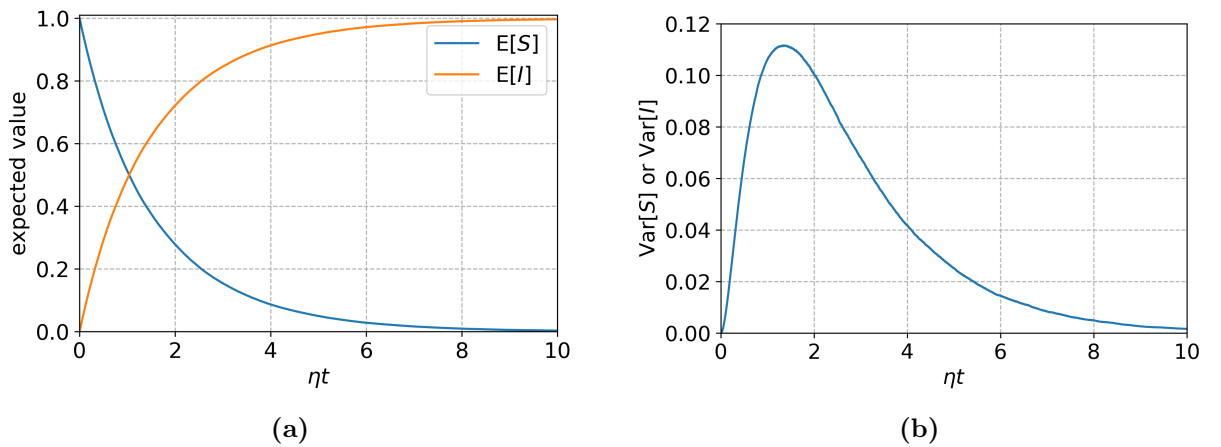


**Figure 3.9:** Expected value and variance of distributions  $P_S(S, t)$  and  $P_I(I, t)$ . Calculations were performed with  $N = 100,000$  samples of Eq. (3.3). We used  $\eta\Delta t = 0.001$  for the time grid.

In Figs. 3.9 we see that the entropy (information gain) evolves from  $S = 1$  ( $I = 0$ ) to

$S = 0$  ( $I = 0$ ) for  $0 \leq \eta t < \infty$ . Fluctuation grows until  $\eta t \approx 1.3$ , attaining its maximum value, to vanish as  $\eta t \rightarrow \infty$ .

By simulating numerous trajectories from (3.3), we determined the probability distributions and average values for the observables of interest for the continuously monitored qubit. However, the question remains whether we can derive a closed form for the probability distributions. The answer is yes, and the theoretical apparatus for its construction is the topic of the next chapter.

# Chapter 4

## Exact solution for quantum trajectories probability distribution

In the preceding chapter, we calculated all the relevant physics of the continuously monitored qubit by numerical integration of the stochastic differential equation (3.1). To perform our calculations, we used  $\Delta t$  sufficiently small to validate the Central Limit Theorem, which allowed us to express the discrete noise in terms of a white Gaussian noise  $\Delta W_n$  distributed according to

$$P_{\text{noise}}(\Delta W_n) \propto e^{-\frac{\Delta W_n^2}{2\eta\Delta t}}.$$

Although each trajectory is stochastic, the probability distribution  $P_q(q, t)$  that arises by considering an infinite number of trajectories is a well-defined function. The same is valid for the distribution of observables  $P_{\mathcal{O}}(\mathcal{O}, t)$  and the moments  $\langle \mathcal{O}^k \rangle$ , for  $k \in \mathbb{N}$ . In this chapter, we will calculate an analytical solution for the continuously measured qubit which will later allow us to obtain the probability distributions (and, consequently, their moments) in a closed form. This is the main contribution of this thesis.

The method's core involves calculating the probability distribution of stochastic trajectory paths described by (2.17). However, we do not directly calculate the path probability distribution for the trajectories  $\{q_n\}$ , but for another variable  $\{Q_n\}$ , where the two paths are related by a non-linear transformation  $q = U(Q)$ . The function  $U$  is chosen in such a way that  $Q$  is described by a Langevin equation with additive (rather than multiplicative) noise. This choice is made to simplify calculations, in particular, to deal with constant mass term that appear into an effective action of the formalis rather than with a variable

mass (which is a much harder problem to solve). Once knowing the stochastic process for the new variable  $Q$ , we construct the path probability distribution  $P[Q]$ . The latter can be expressed in terms of the infinitesimal propagator  $P(Q_{n+1}, t_{n+1}|Q_n, t_n) \equiv P(Q_{n+1}|Q_n)$ , describing the conditional probability for the trajectory being at position  $Q_{n+1}$  at time  $t_{n+1}$ , given its position was  $q_n$  at time  $t_n$ . Therefore, considering the paths as independent from each other, we can write:

$$P[\{Q_n\}] = \prod_{n=0}^{N-1} P(Q_{n+1}|Q_n),$$

where  $N = t/\Delta t$  is the number of partitions of size  $\Delta t$  within the time interval  $t$ . In the continuous limit where  $N \rightarrow \infty$ ,  $\Delta t \rightarrow 0$ , but  $t = N\Delta t$  remains finite, then  $P[\{Q_n\}] \rightarrow P[Q]$ . On which the limit  $\{Q_n\} \rightarrow Q$  is from a discrete to a continuous in-time path. In the end,  $P[Q]$  can be expressed as the product of two factors, that is:

$$P[Q] \stackrel{S}{\equiv} \mathcal{N}[Q]e^{-S[Q]},$$

where  $\mathcal{N}[Q]$  is the measure prefactor, and  $S[Q]$  the action. The index S above the equality is to denote that points of the discrete  $\{Q_n\}$  are to be evaluated at the midpoint before taking the continuous limit.

Once we know  $P[Q]$ , we can compute any average of observables of the form  $\mathcal{O}(q)$ <sup>\*</sup> by the equation:

$$\langle \mathcal{O} \rangle = \frac{\int \mathcal{D}Q P[Q] \mathcal{O}(U(Q))}{\int \mathcal{D}Q P[Q]} \quad (4.1)$$

where

$$\mathcal{D}Q \equiv \lim_{N \rightarrow \infty} \prod_{n=0}^{N-1} d\bar{Q}_n,$$

is the functional measure and  $\bar{Q}_n$  is the midpoint between  $Q_n$  and  $Q_{n+1}$ . The integral  $\int \mathcal{D}Q$  determines a sum over paths in the Feynman sense [44, 45]. The advantage of using Feynman path integral to express the average  $\langle \mathcal{O} \rangle$ , as in Eq. (4.1), is to have a myriad of methods (e.g. saddle point, perturbation theory) from functional integration to test and compare with the numerical data already calculated in chapter 3. For convenience, we will use as a reference the mean purity  $\langle \tau \rangle = \langle \text{tr } \rho^2 \rangle$ , depicted in Fig. 3.6a, to test our theoretical results. We will see that, by using this construction, the saddle point solution

---

<sup>\*</sup>For example,

$$\mathcal{O}(q) = \text{tr } \rho^2 = (1 + q^2)/2$$

for  $P[Q]$  already gives an excellent agreement with the calculated numerical data. The reasoning we will use in the next section to construct  $P[Q]$  closely follows the ideas of [46]. However, we have not found any reference for the analytic solution of the continuously monitored qubit that we will find at the end of this chapter.

## 4.1 Stratonovich Langevin equation without multiplicative noise

Using the Euler-Maruyama method, we numerically integrated the Itô discretized equation:

$$\Delta q = q_{n+1} - q_n = g(q_n)\Delta W_n \quad (4.2)$$

We could perfectly build a path probability distribution  $P[q] = \mathcal{N}[q]e^{-S[q]}$  for  $q$  generated by the equation above. However, the resulting action  $S[q]$  would have a variable mass term  $m(q) = g(q)^{-2}$  [46]. To avoid dealing with a variable mass, we need to perform a change of coordinate  $q = U(Q)$ , such that the Langevin equation describing  $Q$  has additive noise instead of a multiplicative one. But before doing so, because a change of variable of Langevin's Eq. (4.2) involves the use of the stochastic calculus chain rule, it is preferable to work in the Stratonovich (or midpoint) discretization. The reason is that the chain rule is covariant (that is, does not change its form) using the Stratonovich discretization (see appendix B.3 for more detail about the change of discretization of Langevin's equation). When using Stratonovich discretization, the right-hand side of Langevin's equation is evaluated at the midpoint:

$$\bar{q}_n \equiv \frac{q_n + q_{n+1}}{2}.$$

However, because  $\Delta q \sim \mathcal{O}((\eta\Delta t)^{1/2})$  for small  $\Delta t$ , a change of time discretization for Eq. (4.2) yields additional contributions that cannot be ignored. As a result, the Langevin equation evaluated at the midpoint equivalent to Eq. (4.2) is given by:

$$\Delta q = -\frac{g(\bar{q}_n)g'(\bar{q}_n)}{2}\eta\Delta t + g(\bar{q}_n)\Delta W_n + \mathcal{O}((\eta\Delta t)^{3/2}), \quad (4.3)$$

where  $\Delta q = q_{n+1} - q_n$  (see appendix B.2 for details of the derivation of Eq. (4.3)). Now that our Langevin equation is time discretized in the Stratonovich sense, we can perform the change of variable  $q_n = U(Q_n)$  without worrying about extra terms advent from the

stochastic chain's rule. Referring to Eq. (B.17) in the appendix B.4, after the change of variable, Eq. (4.3) will be transformed into:

$$\Delta Q = -\frac{1}{2}g'(U(\bar{Q}_n))\frac{g(U(\bar{Q}_n))}{U'(\bar{Q}_n)}\eta\Delta t + \frac{g(U(\bar{Q}_n))}{U'(\bar{Q}_n)}\Delta W_n + \mathcal{O}((\eta\Delta t)^{3/2}), \quad (4.4)$$

where  $\Delta Q = Q_{n+1} - Q_n$ . To go from Eq. (4.3) to Eq. (4.4), we used the Itô prescription  $\Delta W_n^2 \mapsto \eta\Delta t$ , explained in more detail in the appendix B.1. To eliminate the multiplicative noise from Eq. (4.4), we must choose  $U(Q)$  such that  $U'(Q) = g(U(Q))$ . Therefore:

$$\frac{dU}{dQ} = g(U) = 1 - U^2,$$

thus:

$$\frac{dU}{1 - U^2} = dQ.$$

After integrating both sides from  $Q' = 0$  to  $Q' = Q$ , we obtain:

$$\operatorname{arctanh}(U) - \operatorname{arctanh}(U_0) = Q.$$

Choosing  $U_0 = U(Q = 0) = 0$ , then:

$$U(Q) = \tanh(Q). \quad (4.5)$$

Finally, substituting this equation into Eq. (4.3), we obtain the stochastic process for the variable  $Q$ , described by the following Langevin equation with additive noise:

$$\Delta Q = U(\bar{Q}_n)\eta\Delta t + \Delta W_n + \mathcal{O}((\eta\Delta t)^{3/2}). \quad (4.6)$$

Our original variable  $q$  is described by  $q_n = \tanh(Q_n)$ , at which  $Q_0 = 0$  and  $Q_n$  is a stochastic trajectory obeying by Eq. (4.6).

The error for  $\Delta Q/\Delta t$  given by Eq. (4.6) is of the order  $\mathcal{O}((\eta\Delta t)^{1/2})$ , which is vanishing in the continuous limit, yielding:

$$\frac{dQ}{dt} \stackrel{s}{=} \eta \tanh(Q) + W(t), \quad (4.7)$$

where  $\langle W(t)W(t') \rangle = \eta\delta(t - t')$ . Now we are ready to construct the path probability distribution for  $Q$ .

## 4.2 Path probability distribution

As stated at the beginning of the chapter, the path probability distribution  $P[Q]$ , where  $Q$  is a stochastic trajectory described by Eq. (4.7), is defined by:

$$P[Q] = \lim_{N \rightarrow \infty} \prod_{n=0}^{N-1} P(Q_{n+1}|Q_n) \stackrel{\text{S}}{=} \mathcal{N}[Q] e^{-S[Q]}, \quad (4.8)$$

where  $N = t/\Delta t$ . For simplification, we start by calculating the first step probability distribution  $P(Q_1|Q_0)$  by:

$$P(Q_1|Q_0) = \int d(\Delta W_0) \delta(Q_1 - F(Q_0, \Delta W_0)) P_{\text{noise}}(\Delta W_0), \quad (4.9)$$

where

$$P_{\text{noise}}(\Delta W_0) = \frac{1}{\sqrt{2\pi\eta\Delta t}} e^{-\frac{\Delta W_0^2}{2\eta\Delta t}}, \quad (4.10)$$

and the function  $F(Q_0, \Delta W_0)$  is defined by the equation:

$$\Delta Q - U(\bar{Q}_0)\eta\Delta t - \Delta W_0 \Big|_{Q_1=F(Q_0, \Delta W_0)} = 0, \quad (4.11)$$

with  $\Delta Q = Q_1 - Q_0$  in this context. Since the integral in Eq. (4.9) is over  $\Delta W_0$ , it is more convenient to write the delta function with the noise appearing explicit in its argument.

This can be done using the identity:

$$\delta(f(x)) = \sum_{f(a)=0} \frac{\delta(x-a)}{|f'(x)|}.$$

Therefore, the infinitesimal propagator is rewritten as:

$$P(Q_1|Q_0) = \int d(\Delta W_0) \frac{\delta(\Delta W_0 - G(Q_0, Q_1))}{|\partial_{\Delta W_0} F(Q_0, \Delta W_0)|} P_{\text{noise}}(\Delta W_0),$$

where the function  $G(Q_0, Q_1)$  is defined by equation:

$$Q_1 - F(Q_0, \Delta W_0) \Big|_{\Delta W_0=G(Q_0, Q_1)} = 0. \quad (4.12)$$

Hence, finally:

$$P(Q_1|Q_0) = \frac{P_{\text{noise}}(\Delta W_0)}{|\partial_{\Delta W_0} F(Q_0, \Delta W_0)|} \Big|_{\Delta W_0=G(Q_0, Q_1)}. \quad (4.13)$$

Consequently, to find the expression for  $P(Q_1|Q_0)$ , it suffices to calculate the functions  $F(Q_0, \Delta W_0)$  and  $G(Q_0, Q_1)$ , and plug the result into Eq. (4.13). From Eq. (4.11),



$F(Q_0, \Delta W_0)$  is calculated by solving it explicitly for  $Q_1$ , therefore:

$$\begin{aligned}\Delta Q &= Q_1 - Q_0 = U(\bar{Q}_0)\eta\Delta t + \Delta W_0, \\ &= U\left(Q_0 + \frac{\Delta Q}{2}\right)\eta\Delta t + \Delta W_0, \\ &= U(Q_0)\eta\Delta t + U'(Q_0)\frac{\Delta Q}{2}\eta\Delta t + \Delta W_0 + \mathcal{O}((\eta\Delta t)^2).\end{aligned}$$

Isolating  $\Delta Q$  on the left side, we obtain:

$$\begin{aligned}\Delta Q &= \frac{U(Q_0)\eta\Delta t + \Delta W_0 + \mathcal{O}((\eta\Delta t)^2)}{1 - U'(Q_0)\frac{\eta\Delta t}{2}}, \\ &= \{U(Q_0)\eta\Delta t + \Delta W_0 + \mathcal{O}((\eta\Delta t)^2)\} \left\{1 + U'(Q_0)\frac{\eta\Delta t}{2} + \mathcal{O}((\eta\Delta t)^2)\right\}, \\ &= U(Q_0)\eta\Delta t + \Delta W_0 \left[1 + U'(Q_0)\frac{\eta\Delta t}{2} + \mathcal{O}((\eta\Delta t)^2)\right] + \mathcal{O}((\eta\Delta t)^2).\end{aligned}$$

Therefore:

$$F(Q_0, \Delta W_0) = Q_0 + U(Q_0)\eta\Delta t + \Delta W_0 \left[1 + U'(Q_0)\frac{\eta\Delta t}{2} + \mathcal{O}((\eta\Delta t)^2)\right] + \mathcal{O}((\eta\Delta t)^2). \quad (4.14)$$

Derivating relative to  $\Delta W_0$ , we obtain:

$$\frac{\partial F(Q_0, \Delta W_0)}{\partial \Delta W_0} = 1 + U'(Q_0)\frac{\eta\Delta t}{2} + \mathcal{O}((\eta\Delta t)^2).$$

Thus, the prefactor will be:

$$\begin{aligned}\frac{1}{|\partial_{\Delta W_0} F(Q_0, \Delta W_0)|} &= 1 - U'(Q_0)\frac{\eta\Delta t}{2} + \mathcal{O}((\eta\Delta t)^2) \\ &= \exp\left(-U'(Q_0)\frac{\eta\Delta t}{2} + \mathcal{O}((\eta\Delta t)^2)\right).\end{aligned}$$

Switching back to the midpoint using:

$$Q_0 = \bar{Q}_0 - \frac{\Delta Q}{2},$$

we can finally express the prefactor term by:

$$\frac{1}{|\partial_{\Delta W_0} F|} = \exp\left(-U'(\bar{Q}_0)\frac{\eta\Delta t}{2} + \mathcal{O}((\eta\Delta t)^{3/2})\right). \quad (4.15)$$

We kept explicitly only the linear term in  $\eta\Delta t$ , since higher order terms do not contribute to the path probability distribution in the continuous limit  $\Delta t \rightarrow 0$ . Now, to obtain the function  $G(Q_0, Q_1)$ , we need to solve Eq. (4.12) for  $\Delta W_0$ . Therefore, we have to solve the

following implicit equation for  $G(Q_0, Q_1)$ :

$$\Delta Q - U(Q_0)\eta\Delta t - G(Q_0, Q_1) \left[ 1 + U'(Q_0)\frac{\eta\Delta t}{2} + \mathcal{O}((\eta\Delta t)^2) \right] + \mathcal{O}((\eta\Delta t)^2) = 0.$$

Thus:

$$\begin{aligned} G(Q_0, Q_1) &= \frac{\Delta Q - U(Q_0)\eta\Delta t + \mathcal{O}((\eta\Delta t)^2)}{1 + U'(Q_0)\frac{\eta\Delta t}{2} + \mathcal{O}((\eta\Delta t)^2)}, \\ &= \Delta Q - \left( U(Q_0) - U'(Q_0)\frac{\Delta Q}{2} \right) \eta\Delta t + \mathcal{O}((\eta\Delta t)^2), \\ &= \Delta Q - U(\bar{Q}_0)\eta\Delta t + \mathcal{O}((\eta\Delta t)^2). \end{aligned} \quad (4.16)$$

Finally, the infinitesimal propagator is obtained substituting Eq. (4.15) and Eq. (4.16) into Eq. (4.13), resulting in:

$$\begin{aligned} P(Q_1|Q_0) &= \frac{1}{\sqrt{2\pi\eta\Delta t}} \exp \left\{ -\frac{(\Delta Q - U(\bar{Q}_0)\eta\Delta t + \mathcal{O}((\eta\Delta t)^2))^2}{2\eta\Delta t} - U'(\bar{Q}_0)\frac{\eta\Delta t}{2} + \mathcal{O}((\eta\Delta t)^{3/2}) \right\}, \\ &= \frac{1}{\sqrt{2\pi\eta\Delta t}} \exp \left\{ -\frac{\eta\Delta t}{2} \left( \frac{\Delta Q}{\eta\Delta t} - U(\bar{Q}_0) \right)^2 - \frac{\eta\Delta t}{2} U'(\bar{Q}_0) + \mathcal{O}((\eta\Delta t)^{3/2}) \right\}. \end{aligned}$$

The path probability distribution of a discrete path  $\{Q_n\} = \{Q_0, \dots, Q_N\}$  is calculated by the product of the infinitesimal propagators:

$$P[\{Q_n\}] = \prod_{n=0}^{N-1} P(Q_{n+1}|Q_n).$$

Therefore:

$$P[\{Q_n\}] = (2\pi\eta\Delta t)^{-N/2} \exp \left\{ -\eta\Delta t \sum_{n=0}^{N-1} \left[ \frac{1}{2} \left( \frac{\Delta Q}{\eta\Delta t} - U(\bar{Q}_n) \right)^2 + \frac{U'(\bar{Q}_n)}{2} + \mathcal{O}((\eta\Delta t)^{1/2}) \right] \right\}.$$

Taking the continuous limit  $N \rightarrow \infty$  and  $\Delta t \rightarrow 0$ , where  $N\Delta t = t$ , as stated in Eq. (4.8), we finally obtain the continuous path probability distribution  $P[Q]$ , given by:

$$P[Q] \stackrel{\text{S}}{=} \mathcal{N}[Q] e^{-S[Q]},$$

where

$$\mathcal{N}[Q] = \lim_{N \rightarrow \infty} \left( \frac{N}{2\pi\eta t} \right)^{N/2}, \quad (4.17)$$

is the prefactor contribution, and:

$$S[Q] \stackrel{\text{S}}{=} \int_0^t dt' \left[ \frac{(\dot{Q} - \eta \tanh Q)^2}{2\eta} + \eta \frac{\text{sech}^2 Q}{2} \right],$$

is the action. We made explicit  $U(Q) = \tanh Q$  in  $S[Q]$ . The equation above can be further simplified by the identity  $\operatorname{sech}^2 Q = 1 - \tanh^2 Q$  and expanding the square term  $(\dot{Q} - \eta \tanh Q)^2$ , resulting in:

$$S[Q] \stackrel{\text{S}}{=} \int_0^t dt' \left( \frac{\dot{Q}^2}{2\eta} - \dot{Q} \tanh Q \right). \quad (4.18)$$

The term independent of  $Q$  was absorbed into the prefactor  $\mathcal{N}[Q]$ . Eq. (4.18) is an action with constant mass term  $M = 1$  [47, 45]. Now all the non-trivial dynamics are encoded in the position and velocity-dependent potential:

$$V(Q, \dot{Q}) = -\dot{Q} \tanh Q.$$

† The main contribution to the path probability distribution  $P[Q]$ , is given by the saddle point solution. The saddle point solution is defined by the path (or family of paths) that makes the action stationary, i.e,  $S[Q + \delta Q] = S[Q] + \mathcal{O}(\delta Q^2)$  when  $Q$  is the saddle point solution, where  $\delta Q$  is a small variation of the curve. This point is made more rigorous in the next section, where we will find the curve  $Q$  that extremizes the action.

Before ending this section, we conclude with a last remark: The action  $S[Q]$  written in terms of a general  $\alpha$  discretization:

$$Q_n^\alpha = (1 - \alpha)Q_n + \alpha Q_{n+1},$$

will be given by:

$$S[Q] \stackrel{\alpha}{=} \int_0^t dt' \left[ \frac{(\dot{Q} - \eta U(Q))^2}{2\eta} + \alpha \eta U'(Q) \right], \quad (4.19)$$

where  $U(Q) = \tanh Q$ . Previously we have calculated the special case  $\alpha = \frac{1}{2}$  (Stratonovich discretization). We saw that for this case, we have a cancellation of the  $\tanh^2 Q$  term, which will be essential in the next section for the success of the saddle point solution. For  $\alpha = 0$  (Itô discretization), or any other value of  $\alpha$ , this cancellation does not occur, and the saddle point solution yields a non-integrable equation, which, in addition, does not fully describe the numerical results. More advanced methods are required to obtain an analytical solution for  $\alpha \neq \frac{1}{2}$ .

---

†The minus sign is there because  $S[Q]$  is actually the imaginary time action, defined as:

$$S[Q] = \int dt \left( \frac{M\dot{Q}^2}{2} + V(Q, \dot{Q}) \right)$$

### 4.3 Saddle point solution

The action  $S[Q]$  can be written as:

$$S[Q] \stackrel{\text{S}}{=} \int_0^t dt' L(Q, \dot{Q}), \quad (4.20)$$

where  $L(Q, \dot{Q})$  is a Langrangian given by:

$$L(Q, \dot{Q}) = \frac{\dot{Q}^2}{2\eta} - \dot{Q} \tanh Q. \quad (4.21)$$

Introducing a small variation  $\delta Q$  over the path  $Q$ , the action  $S[Q + \delta Q]$  is given by:

$$\begin{aligned} S[Q + \delta Q] &= \int dt L(Q + \delta Q, \dot{Q} + \delta \dot{Q}) \\ &= \int dt \left\{ L(Q, \dot{Q}) + \frac{\partial L}{\partial Q} \delta Q + \frac{\partial L}{\partial \dot{Q}} \delta \dot{Q} \right\} + \mathcal{O}(\delta Q^2, \delta \dot{Q}^2). \end{aligned}$$

Imposing the constraint that the path variation is null at the initial and final time, i.e., all paths start and end up at the same point in configuration space, the expression above is simplified into:

$$S[Q + \delta Q] = S[Q] + \int dt \left\{ \frac{\partial L}{\partial Q} - \frac{d}{dt} \left( \frac{\partial L}{\partial \dot{Q}} \right) \right\} \delta Q + \mathcal{O}(\delta Q^2).$$

Therefore, if  $Q$  is the saddle point solution we are searching for, it has to satisfy the Euler-Lagrange condition [\[47\]](#):

$$\frac{\partial L}{\partial Q} = \frac{d}{dt} \left( \frac{\partial L}{\partial \dot{Q}} \right). \quad (4.22)$$

Substituting [\(4.21\)](#) into [\(4.22\)](#) yields the following differential equation for  $Q = Q(t)$ :

$$-\dot{Q} \operatorname{sech}^2 Q = \frac{\ddot{Q}}{\eta} - \dot{Q} \operatorname{sech}^2 Q.$$

Consequently  $\ddot{Q} = 0$ . That is an effective free particle. Thus  $\dot{Q} = \Omega$  and  $Q = \Omega t$ , where  $\Omega \in \mathbb{R}$  and has units of inverse time. Hence, the saddle point of the action  $S[Q]$  yields the classical solutions:

$$Q_\Omega = \Omega t,$$

and

$$q_\Omega = \tanh Q_\Omega = \tanh \Omega t.$$

For  $\Omega > 0$  ( $\Omega < 0$ ) the qubit is continuously purified into  $|0\rangle\langle 0|$  ( $|1\rangle\langle 1|$ ). The higher the absolute value of  $\Omega$ , the faster a pure state is obtained. Since there are infinitely many

saddle point solutions labeled by the real parameter  $\Omega$ , all of them have to be summed, weighted by a factor  $\propto e^{-S[Q_\Omega]}$  coming from the path probability distribution  $P[Q_\Omega]$ . Therefore, averages of observables  $\mathcal{O}(q)$  are calculated by the following expression:

$$\begin{aligned}\langle \mathcal{O} \rangle &= \frac{\int_{-\infty}^{\infty} d\Omega \mathcal{O}(\tanh Q_\Omega) e^{-S[Q_\Omega]}}{\int_{-\infty}^{\infty} d\Omega e^{-S[Q_\Omega]}} \\ &= \int_{-\infty}^{\infty} d\Omega P_\Omega(\Omega, t) \mathcal{O}(\tanh \Omega t),\end{aligned}$$

where  $P_\Omega(\Omega, t)$  is the probability distribution of the classical parameter  $\Omega$ , defined by:

$$P_\Omega(\Omega, t) = \frac{e^{-S[Q_\Omega]}}{\int_{-\infty}^{\infty} d\Omega e^{-S[Q_\Omega]}}. \quad (4.23)$$

While  $S[Q_\Omega]$  is the classical action calculated as:

$$\begin{aligned}S[Q_\Omega] &= \int_0^t dt' \left( \frac{\Omega^2}{2\eta} - \Omega \tanh \Omega t' \right) \\ &= \frac{\Omega^2 t}{2\eta} - \ln \cosh \Omega t.\end{aligned}$$

Therefore, the probability distribution for the variable  $\Omega$  is:

$$\begin{aligned}P_\Omega(\Omega, t) &= \frac{e^{-\frac{\Omega^2 t}{2\eta} + \ln \cosh \Omega t}}{\int d\Omega e^{-\frac{\Omega^2 t}{2\eta} + \ln \cosh \Omega t}} \\ &= \left( \frac{\eta t}{2\pi} \right)^{1/2} \exp \left( -\frac{\Omega^2 t}{2\eta} + \ln \cosh \Omega t - \frac{\eta t}{2} \right).\end{aligned} \quad (4.24)$$

Now the mean purity, for example, can be calculated by:

$$\langle \tau \rangle = \int_{-\infty}^{\infty} d\Omega P_\Omega(\Omega, t) \tau(q_\Omega),$$

where  $\tau(q)$  is given by Eq. (3.7) and  $q_\Omega = \tanh \Omega t$ . The result is:

$$\langle \tau \rangle = \frac{1}{2} + \frac{1}{2} \left( \frac{\eta t}{2\pi} \right)^{1/2} \int_{-\infty}^{\infty} d\Omega e^{-\frac{\Omega^2 t}{2\eta} + \ln \cosh \Omega t - \frac{\eta t}{2}} \tanh^2 \Omega t. \quad (4.25)$$

The comparison of  $\langle \tau \rangle$  between the theoretical prediction given by Eq. (4.25) and the numerical result depicted in Fig. 3.6a can be seen in Fig. (4.1) below:

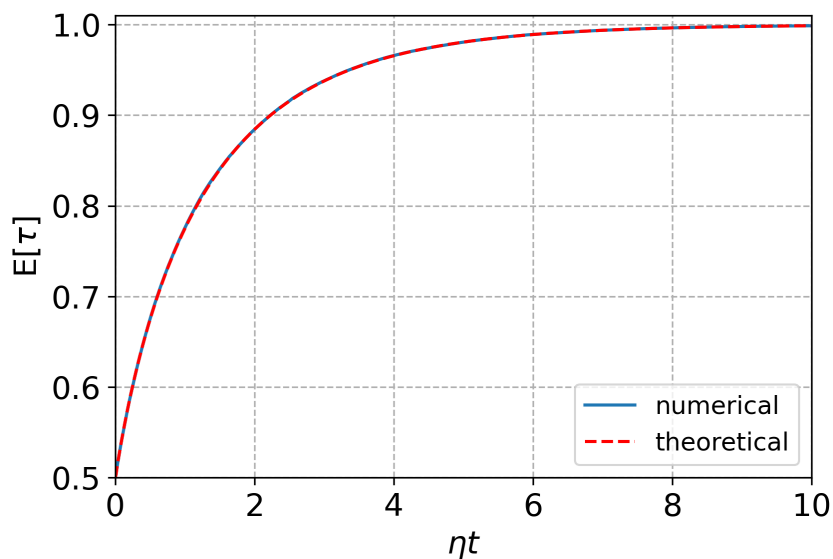


**Figure 4.1:** Mean purity  $E[\tau] = \langle \tau \rangle$ . Comparison between numerical result, calculated by averaging  $\tau(q)$  over 100,000 trajectories generated by Eq. (3.3) (solid blue line) and the theoretical result calculated with Eq. (4.25) (red dashed line)

The agreement is excellent. Remarkably the probability distribution for  $\Omega$  is such that

$$P_{\Omega}(\Omega, t) \rightarrow \frac{\delta(\Omega - \eta) + \delta(\Omega + \eta)}{2},$$

as  $\eta t \rightarrow \infty$ . This tendency is depicted below, where we plotted  $P_{\Omega}(\Omega, t)$  for increasing values of  $t$ :

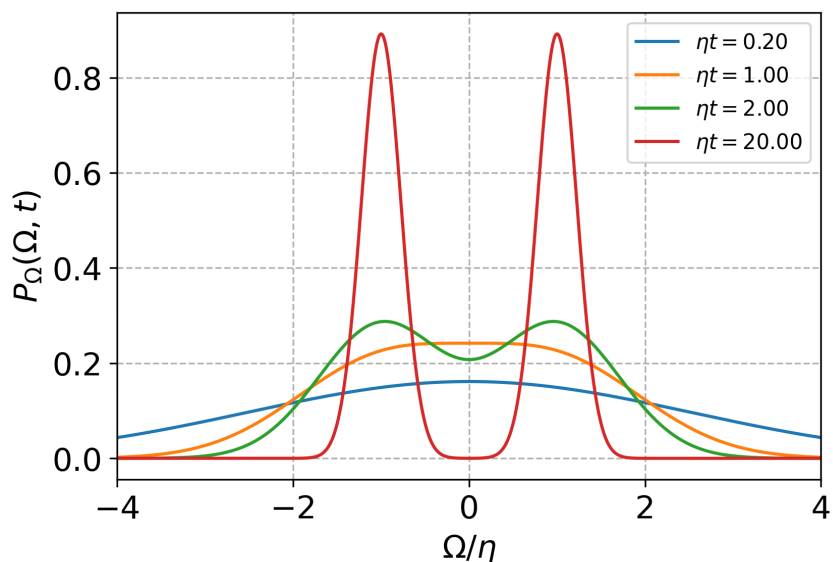


**Figure 4.2:** A plot of  $P_{\Omega}(\Omega, t)$  given by Eq. (4.24) for increasing values of  $t$ .

Therefore, in the limit,  $\eta t \rightarrow \infty$ ,  $P_{\Omega}(\Omega, t)$  tends to a discrete uniform distribution between the values  $\Omega = \pm\eta$ . Each peak is related to the system being purified in one of

the two possible states, since  $q = \tanh \Omega t$ . In figure [4.2](#), we see the appearance of the two peaks for  $P_\Omega(\Omega, t)$  for a threshold of time  $t = t^*$ . They occur with the appearance of a minimum for the classical action

$$S(\Omega, t) = \frac{\Omega^2 t}{2\eta} - \ln \cosh \Omega t, \quad (4.26)$$

for  $\Omega \neq 0$ . More precisely, this minimum occurs when:

$$\left( \frac{\partial S}{\partial \Omega} \right)_t = \frac{\Omega t}{\eta} - t \tanh(\Omega t) = 0.$$

In other words, when the following non-linear equation is solved for  $\Omega$ :

$$\frac{\Omega}{\eta} = \tanh(\Omega t). \quad (4.27)$$

For  $t \rightarrow \infty$ ,  $\Omega = \pm\eta$  is a solution of Eq. [\(4.27\)](#). For finite  $t$ , the values for  $\Omega$  are depicted in the Fig. [4.3](#) below:

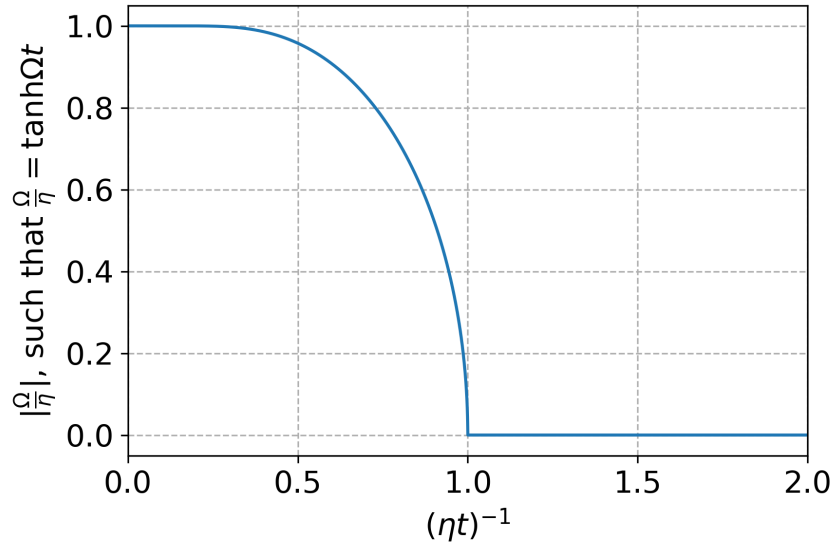


**Figure 4.3:** Solutions of Eq. [\(4.27\)](#) versus  $(\eta t)^{-1}$ .

Therefore, the threshold occurs at  $t^* = \eta^{-1}$ . The action  $S(\Omega, t)$  from Eq. [\(4.26\)](#) is plotted against  $\Omega$  for increasing values of  $t$  in the Fig. [4.4](#) below:

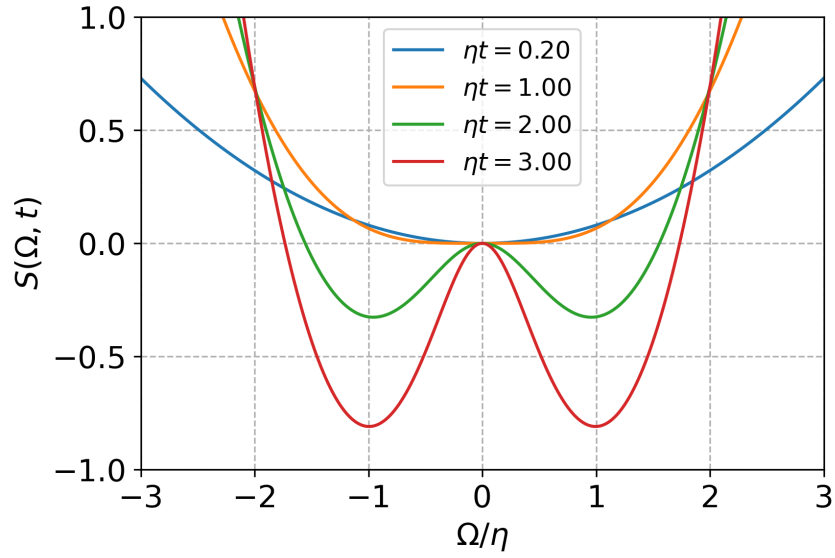


**Figure 4.4:** A plot of the action  $S(\Omega, t)$  from Eq. (4.26) against  $\Omega$  for increasing values of  $t$

From Fig. 4.4, we see that the classical action exhibits a behaviour that resembles a symmetry-broken phenomena, with the average  $\langle |\Omega| \rangle_\Omega$  building from 0 to  $\eta$  as time evolves, where  $\langle \dots \rangle_\Omega \propto \int d\Omega e^{-S(\Omega, t)}(\Omega, t)(\dots)$



# Chapter 5

## Comparison with numerical results

The solution obtained in the previous chapter gave excellent agreement when compared with the numerically calculated mean purity  $\langle \tau \rangle$ , giving confidence in the saddle point solution for the action  $S[Q]$ . We now push the analysis forward, by comparing the predictions of our result with the probability distributions numerically calculated in chapter [3](#). Additionally, our solution allows us to calculate the moments  $\langle \mathcal{O}^k \rangle$ , where  $k \in \mathbb{N}$ , of an observable  $\mathcal{O}$ , in the continuous limit  $\Delta t \rightarrow 0$  and for infinitely many trajectories, using:

$$\langle \mathcal{O}^k \rangle = \int d\mathcal{O} P_{\mathcal{O}}(\mathcal{O}, t) \mathcal{O}^k \quad (5.1)$$

Specifically, we will use Eq. [\(5.1\)](#) to compare our exact solution with the expected values and the variances of the observables considered in chapter [\(3\)](#), namely, the purity, the entropy, and the information gain.

### 5.1 Probability distributions

Once obtained the saddle point solution  $q_{\Omega} = \tanh \Omega t$ , indexed by a real parameter  $\Omega$  distributed by:

$$P_{\Omega}(\Omega, t) = \left( \frac{\eta t}{2\pi} \right)^{1/2} \exp \left( -\frac{\Omega^2 t}{2\eta} + \ln \cosh \Omega t - \frac{\eta t}{2} \right),$$

the probability distribution function (p.d.f)  $P_q(q, t)$  for the position  $q$  is easily obtained by:

$$P_q(q, t) = P_{\Omega}(\Omega(q, t), t) \left| \frac{d\Omega}{dq} \right|.$$

Since  $\Omega = \text{atanh}(q)/t$ , therefore:

$$\begin{aligned} P_q(q, t) &= \frac{P_\Omega(\Omega = \text{atanh}(q)/t, t)}{t(1 - q^2)} \\ &= \frac{1}{\sqrt{2\pi\eta t(1 - q^2)^2}} \exp\left(-\frac{\text{atanh}^2(q)}{2\eta t} + \ln \cosh(\text{atanh}(q)) - \frac{\eta t}{2}\right), \end{aligned} \quad (5.2)$$

where  $-1 \leq q \leq 1$ . Comparison between Eq. (5.2) with the numerical data available in Fig. 3.2 is depicted in Fig. 5.1 below:

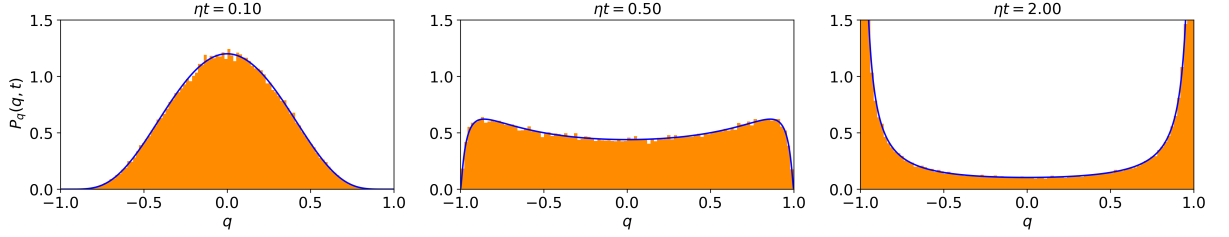


**Figure 5.1:**  $P_q(q, t)$  for  $\eta t = 0.1; 0.5; 2.0$ . Comparison between numerical calculation (orange histograms) and analytical solution given by Eq. (5.2) (solid blue line)

Similarly, we can obtain the p.d.f of an observable  $\mathcal{O} = \mathcal{O}(q)$  by:

$$P_{\mathcal{O}}(\mathcal{O}, t) = P_q(q = f(\mathcal{O}), t) |f'(\mathcal{O})|, \quad (5.3)$$

where  $f$  is the inverse function of  $\mathcal{O}(q)$ , i.e.,  $q = f(\mathcal{O})$ . Therefore, the p.d.f of the purity

$$\tau(q) = \frac{1 + q^2}{2},$$

is given by:

$$\begin{aligned} P_\tau(\tau, t) &= 2 \frac{P_q(q = \sqrt{2\tau - 1}, t)}{\sqrt{2\tau - 1}}, \\ &= \frac{1}{\sqrt{2\pi\eta t(\tau - 1)^2(2\tau - 1)}} \exp\left(-\frac{\text{atanh}^2(\sqrt{2\tau - 1})}{2\eta t} + \ln \cosh(\text{atanh}(\sqrt{2\tau - 1})) - \frac{\eta t}{2}\right), \end{aligned} \quad (5.4)$$

where  $\frac{1}{2} \leq \tau \leq 1$ . The factor 2 take into consideration that  $\tau(q) = \tau(-q)$ . Comparison with the histogram obtained numerically in Fig. 3.5 is depicted in Fig. 5.2 below for increasing values of time:

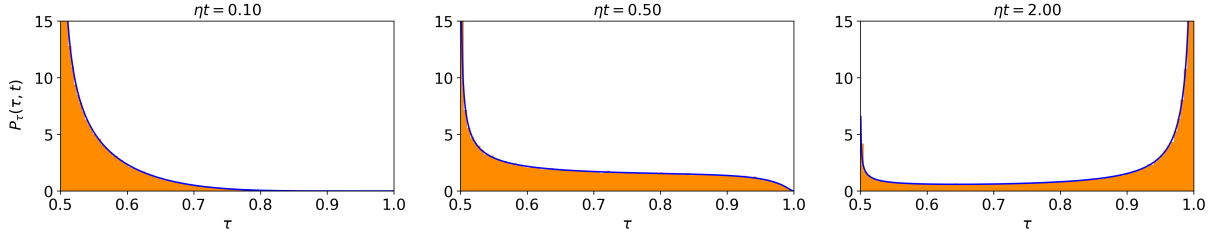


**Figure 5.2:**  $P_\tau(\tau, t)$  for  $\eta t = 0.1; 0.5; 2.0$  units of time. Comparison between numerical calculation (orange histograms) and analytical solution given by Eq. (5.4) (solid blue line)

The PDF for the entropy:

$$S(q) = -\frac{1-q}{2} \log\left(\frac{1-q}{2}\right) - \frac{1+q}{2} \log\left(\frac{1+q}{2}\right), \quad (5.5)$$

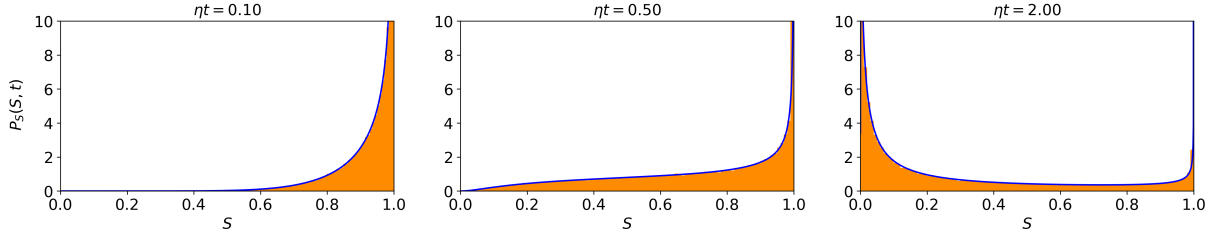
is given by:

$$P_S(S, t) = 2P_q(q = g(S), t)|g'(S)|, \quad \text{where } 0 \leq S \leq 1, \quad (5.6)$$

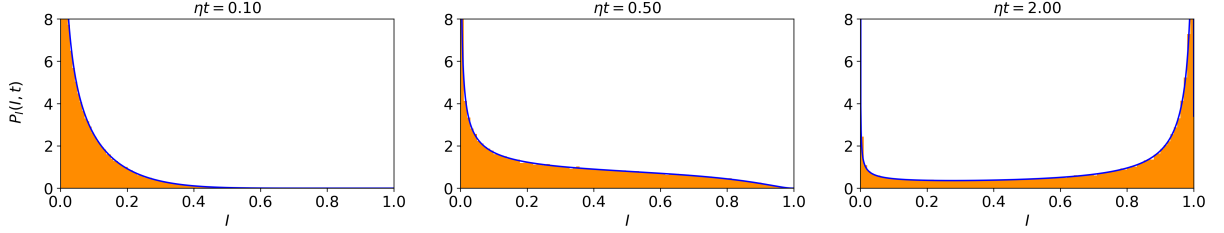
where  $q = g(S)$  in the inverse function of  $S(q)$ . In this case, the function  $g(S)$  was numerically calculated for each value of  $S$  by a root-finding method. Like in Eq. (5.4), factor 2 has to be included because  $S(q) = S(-q)$ . Finally, the information gain  $I(q) = 1 - S(q)$  can be most easily obtained from  $P_S(S, t)$  by:

$$P_I(I, t) = P_S(S = 1 - I, t), \quad \text{where } 0 \leq I \leq 1. \quad (5.7)$$

Comparison between numerical data depicted in Fig. 3.8 and Eqs. (5.6) and (5.7) is in Figs. 5.3 below:



(a)  $P_S(S, t)$  for  $\eta t = 0.1; 0.5; 2.0$ . Comparison between numerical calculation (orange histograms) and analytical solution given by Eq. (5.6) (solid blue line)



(b)  $P_I(I, t)$  for  $\eta t = 0.1; 0.5; 2.0$ . Comparison between numerical calculation (orange histograms) and analytical solution given by Eq. (5.7) (solid blue line)

**Figure 5.3**

From Figs. 5.1, 5.2, and 5.3 we conclude there is an excellent agreement between the theory and numerical calculations. This greatly increases confidence in the saddle point solution obtained in section 4.3.

## 5.2 Averages and fluctuations

After obtaining the probability distribution for the observable  $\mathcal{O}$ , we can compute any moment of order  $k$  by:

$$\langle \mathcal{O}^k \rangle = \int d\mathcal{O} P_{\mathcal{O}}(\mathcal{O}, t) \mathcal{O}^k. \quad (5.8)$$

In particular, Eq. (5.8) can be used to calculate the expected value  $E[\mathcal{O}] = \langle \mathcal{O} \rangle$  and the variance  $\text{Var}[\mathcal{O}] = \langle \mathcal{O}^2 \rangle - \langle \mathcal{O} \rangle^2$ , which are our primary interest in this section.

Using Eq. (5.4), we calculated the expected value and variance for the purity  $\tau(q)$ . Comparison between theory and numerical results from Fig. 3.6 are below:

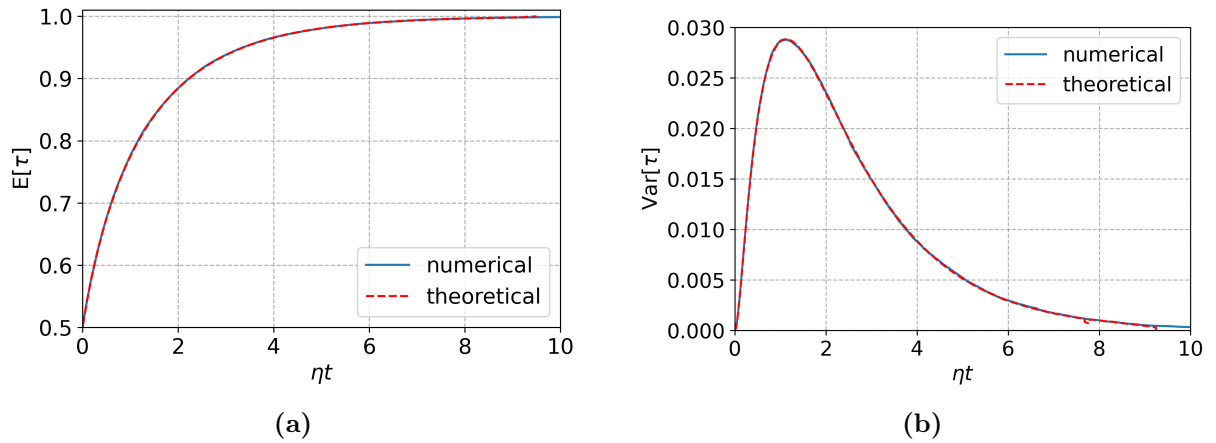


**Figure 5.4:** Comparison between analytical solution (red dashed line) and numerical result (blue solid line) for the expected value (left) and variance (right) for the purity  $\tau$

Here, calculations were performed only up to  $\eta t = 9.5$ . Beyond this, numerical integration of (5.8) becomes unstable due to the singularity of the distribution  $P_\tau(\tau, t)$  at  $\tau = 1$ .

We also compared analytical solutions for the mean and variance with numerical findings for the entropy and information gain. The result is depicted in Figs. 5.5 below:

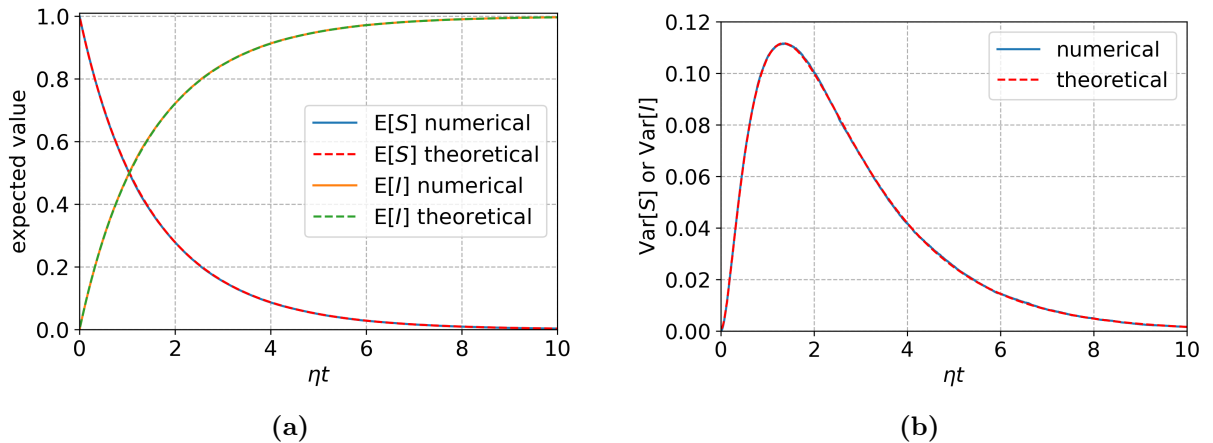


**Figure 5.5:** Comparison between analytical solution (dashed lines) and numerical result (solid lines) for the expected value (left) and variance (right) of the entropy  $S$  and the information gain  $I$

As expected from the previous section, where we found a very good agreement for the probability distributions, the same occurs for the expected value and the variance of the observables considered, as is evident from Figs. 5.4 and 5.5.

# Chapter 6

## Conclusions

We studied the hybrid dynamics of single qubit weakly coupled to ancillary qubits prepared in the same state, with the latter being monitored at a constant rate. As a result, the effective dynamics for the system is of a *continuously monitored qubit*. Starting the system in a mixed state, we showed that the density matrix time evolution depends on a single parameter  $q = q(t)$ . This parameter evolves according to a stochastic differential equation with multiplicative Gaussian white noise, i.e., a *Langevin equation*. The noise accounts for the measurement over the ancilla outcomes, with its amplitude modulated by the function  $g(q) = 1 - q^2$  (multiplicative noise). By numerical integration of the Langevin equation (Euler-Maruyama method), we could calculate precise curves for the average behavior and probability distributions of the purity, the Von-Neumann entropy, and the information gain. An analytical solution was obtained by constructing a path probability distribution for the Langevin equation in the configuration space (Onsager-Machlup path integral). To simplify the calculation, we changed discretization from Ito to Stratonovich discretization, and we also changed the variable by a non-linear mapping  $q = \tanh Q$  to deal with an action with a constant mass term for  $Q$ . An analytical solution was obtained using the saddle point approximation for the path probability distribution  $P[Q] \propto e^{-S[Q]}$ . This statement is well-supported by the excellent agreement between numerical calculations and analytical prediction for the average behavior and probability distributions for the state parameter  $q = q(t)$ , the entropy, the purity, and the information gain.

A surprising finding is the two peak structures for the purification distributions, a feature that appears in the purity and the entropy distributions. Intuitively one would expect a single peak with its maximum value running continuously over time from  $S = 1$

to  $S = 0$  as the qubit is monitored, where  $S$  is the Von-Neumann entropy with base two for the logarithm. However, that is not the case obtained from numerics and the analytical solution. The distribution has a discontinuous feature, where, starting with a peak at  $S = 1$ , another peak at  $S = 0$  rapidly appears, growing over time, until the contributions of the pure state dominate. Therefore, by continuously monitoring the system, the purification appears to occur more abruptly than one would expect.

Although the problem of a continuously monitored qubit allows a relatively simple analytical solution for the average behavior of the qubit replicas, it is unfortunate a too simple model to see a measured induced phase transition. Having established the Onsager-Machlup functional integral for the simplest case, it is natural, therefore, to consider a more complex variant of the problem. The next step would be coupling the continuously monitored qubit considered in this thesis with a scrambling process, e.g., a quantum dot described by a random matrix. By tuning the measurement rate, we would expect to see a phase transition between an ergodic and a localized phase below and above a critical rate, respectively.

# Appendix A

## Non-unitary diffusion Master Equation using POVM's

Measurements in quantum mechanics are usually described by a set of projective operators  $\{\mathcal{P}_n\}$ , such that  $\mathcal{P}_n\mathcal{P}_m = \mathcal{P}_n\delta_{n,m}$  (orthogonality), and  $\mathcal{P}_n^\dagger = \mathcal{P}_n$  (Hermitian property). If the system is in the state  $\rho$ , after a projective measurement, the system will be in the state

$$\rho' = \frac{\mathcal{P}_n\rho\mathcal{P}_n}{p_n},$$

where  $p_n = \text{tr}(\mathcal{P}_n\rho)$  is the probability of the outcome labeled by  $n$  to occur [39, 36, 35]. For the particular case of projective measurement over the eigenstates of  $\sigma_z$ , the projective operators are  $\mathcal{P}_0 = |0\rangle\langle 0|$  and  $\mathcal{P}_1 = |1\rangle\langle 1|$ , where  $\sigma_z|0\rangle = |0\rangle$  and  $\sigma_z|1\rangle = -|1\rangle$ . However, this is not the most general set of measurement operators. A measurement that extracts partial information about a system cannot be described by the set  $\{\mathcal{P}_n\}$ , since the projective operator can only return full information of the outcome when directly applied.

An extension is done using *Positive Operators Valued Measurement* (POVM). POVMs are described by the set of operators  $\{\Omega_n\}$ , such that

$$\sum_n \Omega_n^\dagger \Omega_n = \hat{1}. \quad (\text{A.1})$$

If the system is in the state  $\rho$ , after measurement by a POVM the system will be in the state

$$\rho' = \frac{\Omega_n\rho\Omega_n^\dagger}{p_n},$$



where  $p_n = \text{tr}(\Omega_n \rho \Omega_n^\dagger)$  is the probability of the outcome labeled by  $n$ . Notice that Eq. (A.1) guarantees that  $\sum_n p_n = 1$ . In particular, if  $\Omega_n^\dagger = \Omega_n$  and  $\Omega_n^\dagger \Omega_m = \Omega_n \delta_{n,m}$ , we get back projective measurements. So POVMs are more general than projective measurements. To arrive at equation (2.11) using POVM, one must use that

$$\rho_{t+dt} = \frac{\Omega_n \rho_t \Omega_n^\dagger}{p_n},$$

where:

$$\begin{aligned}\Omega_0 &= \frac{1}{\sqrt{2}} (|0\rangle\langle 0| + (\cos \theta - \sin \theta) |1\rangle\langle 1|), \\ \Omega_1 &= \frac{1}{\sqrt{2}} (|0\rangle\langle 0| + (\cos \theta + \sin \theta) |1\rangle\langle 1|),\end{aligned}$$

with  $\theta = \sqrt{dt} \ll 1$  [35]. As was done in section 2.1, the two possible evolutions for the state  $\rho_t$  can be cast into a single equation by the introduction of a stochastic variable  $dW = \pm\sqrt{dt}$  with equal probability for each outcome.

# Appendix B

## Basic notions of Stochastic calculus

In 1908, Paul Langevin proposed a dynamic equation that correctly described the erratic motion of a macroscopic particle embedded in a solvent, such as the motion of a pollen grain suspended in a liquid, also known as the Brownian Motion [48]. Although Einstein already explained Brownian motion by deducing a diffusion equation for the suspended particle (known today as the Fokker-Planck equation) [49, 50], Langevin's description is more intuitive and easily generalized. Its originality was to propose a stochastic differential equation (SDE) to describe physical phenomena. In its general form, the one-dimensional Langevin equation is

$$\frac{dx}{dt} \stackrel{\alpha}{=} f(x) + g(x)W(t), \quad (\text{B.1})$$

where  $W(t)$  is a gaussian white noise with  $\langle W(t)W(t') \rangle = 2D\delta(t - t')$ ,  $D$  is the diffusion coefficient, and  $f(x)$  is a drift force. If  $g'(x) \neq 0$ , we say that Eq. (B.1) has a multiplicative noise, otherwise, we define it as an SDE with additive noise. The bridge between Langevin's and Einstein's solution [49] to the Brownian motion is given by the Fokker-Planck equation:

$$\frac{\partial}{\partial t}p(x, t) = -\frac{\partial}{\partial x}(f(x)p(x, t)) + D\frac{\partial^2}{\partial x^2}(g(x)^2p(x, t)), \quad (\text{B.2})$$

which describes the probability distribution  $p(x, t)$  of many trajectories generated by Eq. (B.1). An initial configuration is specified by  $p(x, 0) = \mathcal{F}(x)$ . However, to simulate the trajectories and compare them with the probability distribution  $p(x, t)$ , a discretization scheme has to be specified. This is the role of the index  $\alpha$  above the equality, a point that is discussed in more detail in the next section.

## B.1 Discrete-time stochastic differential equation and Itô's rule

Stochastic differential equations with multiplicative noise, such as Eq. (B.1), are ambiguous without specifying the discretization scheme used before taking the continuous limit  $\Delta t \rightarrow 0$ . To lift the ambivalence, a proper time discretization scheme has to be defined. This can be realized by dividing the time interval of size  $t$  into  $N$  equal parts  $\Delta t = t/N$ . Time is now defined by  $t_n = n\Delta t$ , where  $n = 0, 1, \dots, N$ . Likewise, we define position by  $x_n \equiv x(t_n)$ . Therefore, Eq. (B.1) discrete form will be

$$\frac{\Delta x}{\Delta t} = f(x_n^\alpha) + g(x_n^\alpha)W_n, \quad (\text{B.3})$$

where  $\Delta x = x_{n+1} - x_n$ ,

$$\langle W_n W_{n'} \rangle = 2D\delta_{n,n'}/\Delta t, \quad (\text{B.4})$$

and

$$x_n^\alpha = (1 - \alpha)x_n + \alpha x_{n+1}.$$

The index  $\alpha \in [0, 1]$  accounts for the chosen discretization. The most common choices are  $x_n^{\alpha=0} = x_n$ , also known as Itô discretization, and

$$x_n^{\alpha=1/2} \equiv \bar{x}_n = \frac{x_n + x_{n+1}}{2},$$

known as the midpoint or Stratonovich discretization. The Itô scheme has the advantage that noise and position are not locally correlated in time. This is convenient for the construction of stochastic path integrals and numerical simulation. On the other hand, Stratonovich discretization is more suited than Itô's when a change of variable has to be performed since the chain rule of ordinary calculus preserves its form when using this scheme.

The reason why the continuous limit is ambiguous when a discretized scheme is not specified, like in Eq. (B.1), lies from the fact that  $\Delta x \sim \mathcal{O}(\Delta t^{1/2})$  as  $\Delta t \rightarrow 0$  <sup>\*</sup>. This is the main difference between a stochastic trajectory and a deterministic one, where  $\Delta x \sim \mathcal{O}(\Delta t)$ . As a consequence, stochastic trajectories, such as the path taken by a Brownian particle, are nowhere differentiable, since the limit  $\Delta x/\Delta t \rightarrow \infty$  as  $\Delta t \rightarrow 0$

---

<sup>\*</sup>This is easily deduced from Eq. (B.3), by noticing that  $W_n \sim \mathcal{O}(\Delta t^{-1/2})$

at every point of the trajectory. It took more than 40 years after Langevin proposed his equation for the invention of stochastic calculus by the Japanese mathematician Kiyosi Itô [51].

From the physicist's viewpoint, the rules of ordinary calculus at the Langevin equation can be maintained, provided one is careful to keep the relevant terms and use Itô's substitution rule:

$$\Delta x^2 \mapsto 2Dg(x_n^\alpha)\Delta t, \quad (\text{B.5})$$

for when  $x$  obeys Eq. (B.3). Or equivalently:

$$W_n^2\Delta t \mapsto 2D, \quad (\text{B.6})$$

for a white noise where  $\langle W_n W_{n'} \rangle = 2D\Delta t^{-1}\delta_{n,n'}$ . These prescriptions are to be understood in the  $L^2$ -norm sense, not as a point-wise equality. For example, in the case of the rule (B.5), the mapping underlying meaning is that:

$$\left\langle \left[ \int_0^t dt' \left( \frac{\Delta x^2}{\Delta t} - 2Dg(x_n^\alpha) \right) \right]^2 \right\rangle = 0 \quad \text{as} \quad \Delta t \rightarrow 0 \quad \text{for all} \quad t \geq 0, \quad (\text{B.7})$$

where average is calculated over many stochastic realizations of Eq. (B.3). This condition is sufficient to use the prescription (B.5) without changing the probability distribution of the stochastic process, but not enough to keep the trajectories unchanged for the same noise realization. More details can be found in Ref. [46] appendix.

The use of Itô's rule will be exemplified in the next two sections, where a change of discretization and a change of variable is performed for Eq. (B.3), respectively.

## B.2 Change of discretization

Let be the following Langevin equation:

$$\frac{dx}{dt} \stackrel{\alpha}{=} f(x) + g(x)W(t), \quad (\text{B.8})$$

which is equivalent to stating that:

$$\frac{\Delta x}{\Delta t} = f(x_n^\alpha) + g(x_n^\alpha)W_n, \quad (\text{B.9})$$

for

$$x_n^\alpha = (1 - \alpha)x_n + \alpha x_{n+1} = x_n + \alpha \Delta x,$$

and  $\langle W_n W_{n'} \rangle = 2D\delta_{n,n'}/\Delta t$ . We want to perform a change of discretization from  $x_n^\alpha \rightarrow x_n^\beta = x_n + \beta \Delta t$ . The relation between the two discretizations is given by

$$x_n^\alpha = x_n^\beta + (\alpha - \beta)\Delta x.$$

Substituting this last relation into Eq. (B.9) and Taylor expanding up to first order in  $\Delta x$ , we obtain:

$$\begin{aligned} \frac{\Delta x}{\Delta t} &= f(x_n^\beta + (\alpha - \beta)\Delta x) + g(x_n^\beta + (\alpha - \beta)\Delta x)W_n \\ &= f(x_n^\beta) + g(x_n^\beta)W_n + (\alpha - \beta)g'(x_n^\beta)\Delta x W_n + \mathcal{O}(\Delta t^{1/2}). \end{aligned}$$

Where we used  $\Delta x \sim \mathcal{O}(\Delta t^{1/2})$  in the last step. Substituting Eq. (B.9) on the right-hand side of this expression, we get:

$$\frac{\Delta x}{\Delta t} = f(x_n^\beta) + g(x_n^\beta)W_n + (\alpha - \beta)g'(x_n^\beta)g(x_n^\alpha)\Delta t W_n^2 + \mathcal{O}(\Delta t^{1/2}).$$

Using Itô's rule  $\Delta t W_n^2 \mapsto 2D$  and realizing that  $g(x_n^\alpha) = g(x_n^\beta) + \mathcal{O}(\Delta t^{1/2})$ , we finally obtain:

$$\frac{\Delta x}{\Delta t} = f(x_n^\beta) + 2D(\alpha - \beta)g'(x_n^\beta)g(x_n^\beta) + g(x_n^\beta)W_n + \mathcal{O}(\Delta t^{1/2}).$$

After taking the continuous limit, the result is:

$$\frac{dx}{dt} \stackrel{\beta}{=} f_{\alpha \rightarrow \beta}(x) + g(x)W(t), \quad (\text{B.10})$$

where:

$$f_{\alpha \rightarrow \beta} = f(x) + 2D(\alpha - \beta)g'(x)g(x). \quad (\text{B.11})$$

Consequently, we can draw the following rule of equivalence between discretization schemes:

$$\frac{dx}{dt} \stackrel{\alpha}{=} f(x) + g(x)W(t) \Leftrightarrow \frac{dx}{dt} \stackrel{\beta}{=} f_{\alpha \rightarrow \beta}(x) + g(x)W(t). \quad (\text{B.12})$$

With  $f_{\alpha \rightarrow \beta}(x)$  given by Eq. (B.11). The equivalence (B.12) between different discretization schemes is not in the sense of equality, where the trajectories will coincide point to point in time, as was pointed out in the previous section. What Eq. (B.8) and (B.10) share is the same probability distribution, described by a Fokker-Planck equation [46, 52].

From the equivalence (B.12), it is clear why a discretization scheme has to be specified

in the presence of a multiplicative noise. Changing discretization in the Langevin equation yields the additional drift term  $\propto g'(x)g(x)$ . For the additive noise case, i.e. when  $g'(x) = 0$ , the change of discretization has no effect in the continuous limit. Consequently, all discretizations will yield the same form of the Langevin equation. However, with multiplicative noise,  $g'(x) \neq 0$ , hence time discretization has to be specified.

As a particular application of the rule (B.12), starting with a Itô discretized Langevin equation described by

$$\frac{dx}{dt} \stackrel{\text{I}}{=} f(x) + g(x)W(t).$$

The equivalent Stratonovich discretized Langevin equation will be

$$\frac{dx}{dt} \stackrel{\text{S}}{=} f(x) - Dg'(x)g(x) + g(x)W(t),$$

where "I" and "S" above the equal sign mean  $\alpha = 0$  and  $\alpha = 1/2$ , respectively.

### B.3 The stochastic chain rule

In deterministic calculus, when performing the change of variable  $y = h(x)$ , where  $h$  is a smooth function of  $x$ , the rate of change  $dy/dt$  is calculated by the chain rule:

$$\frac{dy}{dt} = \frac{dy}{dx} \frac{dx}{dt} = h'(x) \frac{dx}{dt}. \quad (\text{B.13})$$

This is a well-known result and can be found in any introductory calculus textbook. However, if  $x$  is a stochastic variable obeying a Langevin equation such as Eq. (B.9), the chain rule above is not necessarily true anymore. We will show that Eq. (B.13) holds for the Stratonovich discretization, but an additional term has to be considered for other discretization schemes.

Let  $x$  be a stochastic variable described by the equation:

$$\frac{dx}{dt} \stackrel{\alpha}{=} f(x) + g(x)W(t).$$

If we perform the change of variable  $y = h(x)$ , the increment  $\Delta y = y_{n+1} - y_n$  as a function of  $x$  is given by:

$$\Delta y = h(x_{n+1}) - h(x_n) = h(x_n^\alpha + (1 - \alpha)\Delta x) - h(x_n^\alpha - \alpha\Delta x).$$

Taylor expanding the function  $h$  around  $x_n^\alpha$ , we obtain:

$$\Delta y = h'(x_n^\alpha)\Delta x + \left(\frac{1}{2} - \alpha\right) h''(x_n^\alpha)\Delta x^2 + \mathcal{O}(\Delta x^3) \quad (\text{B.14})$$

Since  $\Delta x \sim \mathcal{O}(\Delta t^{1/2})$ , we had to expand up to  $\Delta x^2 \sim \mathcal{O}(\Delta t)$ , because it is a relevant term for  $\Delta y/\Delta t$ . From Itô's rule (see Eq. (B.6)), we have that

$$\Delta x^2 = 2Dg^2(x_n^\alpha)\Delta t + \mathcal{O}(\Delta t^{3/2}),$$

which when substituted in Eq. (B.14), gives:

$$\Delta y = h'(x_n^\alpha)\Delta x + 2D\left(\frac{1}{2} - \alpha\right) h''(x_n^\alpha)g^2(x_n^\alpha)\Delta t + \mathcal{O}(\Delta t^{3/2}).$$

Dividing it by  $\Delta t$  and taking the continuous limit  $\Delta t \rightarrow 0$ , we finally obtain the stochastic chain rule for  $y = h(x)$ , that is:

$$\frac{dy}{dt} \stackrel{\alpha}{=} h'(x)\frac{dx}{dt} + 2D\left(\frac{1}{2} - \alpha\right) h''(x)g^2(x). \quad (\text{B.15})$$

Surprisingly, for  $\alpha = \frac{1}{2}$  (Stratonovich discretization), the chain rule of deterministic calculus is valid, even though  $x$  is a nowhere differentiable function! Therefore, the chain rule is covariant when Stratonovich discretization is used.

## B.4 Change of variable in Langevin equation

Having established the stochastic chain rule in the preceding section with Equation (B.15), we can now apply this understanding to derive Langevin's equation for  $y = h(x)$ , where  $x$  is described by:

$$\frac{dx}{dt} \stackrel{\alpha}{=} f(x) + g(x)W(t). \quad (\text{B.16})$$

Because of the covariance of the chain's rule for the Stratonovich discretization, let's restrict ourselves to  $\alpha = \frac{1}{2}$ . Supposing the existence of the inverse of  $h$ , then  $x = U(y)$ , where  $U = h^{-1}$ . Consequently:

$$\frac{dx}{dt} \stackrel{\text{S}}{=} U'(y)\frac{dy}{dt}.$$

Substituting this expression into Eq. (B.16), we get:

$$U'(y)\frac{dy}{dt} \stackrel{\text{S}}{=} f(U(y)) + g(U(y))W(t).$$

So Langevin's equation for  $y$ , will be

$$\frac{dy}{dt} \stackrel{\text{s}}{=} \frac{f(U(y))}{U'(y)} + \frac{g(U(y))}{U'(y)}W(t). \quad (\text{B.17})$$

Using the equivalence relation [\(B.12\)](#) together with Eq. [\(B.17\)](#), we can obtain Langevin's equation of the variable  $y$  for any discretization scheme.

A particularly interesting choice for  $U(y)$  occurs when  $U'(y) = g(U(y))$ . In this case, the function  $U(y)$  can be found by solving the integral equation:

$$\int_{U_0}^{U(y)} \frac{dU}{g(U)} = y - y_0, \quad (\text{B.18})$$

where  $U_0 = U(y_0)$ . Consequently, we obtain an additive noise stochastic differential equation for  $y$ , namely:

$$\frac{dy}{dt} \stackrel{\text{s}}{=} \frac{f(U(y))}{g(U(y))} + W(t)$$



# Bibliography

- [1] D S Fisher, Adam Nahum, and S Vijay. “Random Quantum Circuits”. In: *Annual Review of Condensed Matter Physics* 11 (2020), pp. 123–146.
- [2] J. M. Deutsch. “Quantum statistical mechanics in a closed system”. In: *Phys. Rev. A* 43 (4 Feb. 1991), pp. 2046–2049. DOI: [10.1103/PhysRevA.43.2046](https://doi.org/10.1103/PhysRevA.43.2046). URL: <https://link.aps.org/doi/10.1103/PhysRevA.43.2046>.
- [3] Mark Srednicki. “Chaos and quantum thermalization”. In: *Phys. Rev. E* 50 (2 Aug. 1994), pp. 888–901. DOI: [10.1103/PhysRevE.50.888](https://doi.org/10.1103/PhysRevE.50.888). URL: <https://link.aps.org/doi/10.1103/PhysRevE.50.888>.
- [4] Marcos Rigol, Vanja Dunjko, and Maxim Olshanii. “Thermalization and its mechanism for generic isolated quantum systems”. In: *Nature* 452 (2008), pp. 854–858. DOI: [10.1038/nature06838](https://doi.org/10.1038/nature06838). URL: <https://doi.org/10.1038/nature06838>.
- [5] Don N. Page. “Average entropy of a subsystem”. In: *Phys. Rev. Lett.* 71 (9 Aug. 1993), pp. 1291–1294. DOI: [10.1103/PhysRevLett.71.1291](https://doi.org/10.1103/PhysRevLett.71.1291). URL: <https://link.aps.org/doi/10.1103/PhysRevLett.71.1291>.
- [6] Patrick Hayden and John Preskill. “Black holes as mirrors: Quantum information in random subsystems”. In: *Journal of High Energy Physics* 2007 (Sept. 2007). DOI: [10.1088/1126-6708/2007/09/120](https://doi.org/10.1088/1126-6708/2007/09/120).
- [7] J.L.F. Barbón and J.M. Magán. “Fast scramblers, horizons and expander graphs”. In: *J. High Energ. Phys.* 2012.16 (2012), p. 16. DOI: [10.1007/JHEP08\(2012\)016](https://doi.org/10.1007/JHEP08(2012)016). URL: [https://doi.org/10.1007/JHEP08\(2012\)016](https://doi.org/10.1007/JHEP08(2012)016).
- [8] Winton Brown and Omar Fawzi. *Scrambling speed of random quantum circuits*. 2013. arXiv: [1210.6644 \[quant-ph\]](https://arxiv.org/abs/1210.6644).

- [9] N. Lashkari et al. “Towards the fast scrambling conjecture”. In: *J. High Energ. Phys.* 2013.22 (2013), p. 22. DOI: [10.1007/JHEP04\(2013\)022](https://doi.org/10.1007/JHEP04(2013)022). URL: [https://doi.org/10.1007/JHEP04\(2013\)022](https://doi.org/10.1007/JHEP04(2013)022).
- [10] Rahul Nandkishore and David A. Huse. “Many-Body Localization and Thermalization in Quantum Statistical Mechanics”. In: *Annual Review of Condensed Matter Physics Physics* 6.1 (Mar. 2015), pp. 15–38. ISSN: 1947-5462. DOI: [10.1146/annurev-conmatphys-031214-014726](https://doi.org/10.1146/annurev-conmatphys-031214-014726). URL: <http://dx.doi.org/10.1146/annurev-conmatphys-031214-014726>.
- [11] Ehud Altman and Ronen Vosk. “Universal Dynamics and Renormalization in Many-Body-Localized Systems”. In: *Annual Review of Condensed Matter Physics* (2015), pp. 383–409. ISSN: 1947-5462. DOI: [10.1146/annurev-conmatphys-031214-014701](https://doi.org/10.1146/annurev-conmatphys-031214-014701).
- [12] Niklas Bölter and Stefan Kehrein. “Scrambling and many-body localization in the XXZ chain”. In: *Phys. Rev. B* 105 (10 Mar. 2022), p. 104202. DOI: [10.1103/PhysRevB.105.104202](https://doi.org/10.1103/PhysRevB.105.104202). URL: <https://link.aps.org/doi/10.1103/PhysRevB.105.104202>.
- [13] Amos Chan et al. “Unitary-projective entanglement dynamics”. In: *Phys. Rev. B* 99 (22 June 2019), p. 224307. DOI: [10.1103/PhysRevB.99.224307](https://doi.org/10.1103/PhysRevB.99.224307). URL: <https://link.aps.org/doi/10.1103/PhysRevB.99.224307>.
- [14] Yaodong Li, Xiao Chen, and Matthew P. A. Fisher. “Quantum Zeno effect and the many-body entanglement transition”. In: *Phys. Rev. B* 98 (20 Nov. 2018), p. 205136. DOI: [10.1103/PhysRevB.98.205136](https://doi.org/10.1103/PhysRevB.98.205136). URL: <https://link.aps.org/doi/10.1103/PhysRevB.98.205136>.
- [15] Brian Skinner, Jonathan Ruhman, and Adam Nahum. “Measurement-Induced Phase Transitions in the Dynamics of Entanglement”. In: *Phys. Rev. X* 9 (3 July 2019), p. 031009. DOI: [10.1103/PhysRevX.9.031009](https://doi.org/10.1103/PhysRevX.9.031009). URL: <https://link.aps.org/doi/10.1103/PhysRevX.9.031009>.
- [16] Yaodong Li, Xiao Chen, and Matthew P. A. Fisher. “Measurement-driven entanglement transition in hybrid quantum circuits”. In: *Phys. Rev. B* 100 (13 Oct. 2019), p. 134306. DOI: [10.1103/PhysRevB.100.134306](https://doi.org/10.1103/PhysRevB.100.134306). URL: <https://link.aps.org/doi/10.1103/PhysRevB.100.134306>.

- [17] Romain Vasseur et al. “Entanglement transitions from holographic random tensor networks”. In: *Phys. Rev. B* 100 (13 Oct. 2019), p. 134203. DOI: [10.1103/PhysRevB.100.134203](https://doi.org/10.1103/PhysRevB.100.134203). URL: <https://link.aps.org/doi/10.1103/PhysRevB.100.134203>.
- [18] Dorit Aharonov. “Quantum to classical phase transition in noisy quantum computers”. In: *Phys. Rev. A* 62 (6 Nov. 2000), p. 062311. DOI: [10.1103/PhysRevA.62.062311](https://doi.org/10.1103/PhysRevA.62.062311). URL: <https://link.aps.org/doi/10.1103/PhysRevA.62.062311>.
- [19] Béla Bollobás and Oliver Riordan. *Percolation*. New York: Cambridge University Press, 2006.
- [20] Geoffrey Grimmett. *Percolation*. 2nd. Berlin: Springer-Verlag, 1999.
- [21] Kim Christensen. *Percolation Theory*. 2002. URL: [http://www.mit.edu/~levitov/8.334/notes/percol\\_notes.pdf](http://www.mit.edu/~levitov/8.334/notes/percol_notes.pdf).
- [22] Yaodong Li, Xiao Chen, and Matthew P. A. Fisher. “Measurement-driven entanglement transition in hybrid quantum circuits”. In: *Phys. Rev. B* 100 (13 Oct. 2019), p. 134306. DOI: [10.1103/PhysRevB.100.134306](https://doi.org/10.1103/PhysRevB.100.134306). URL: <https://link.aps.org/doi/10.1103/PhysRevB.100.134306>.
- [23] Kemal Aziz, Ahana Chakraborty, and J. H. Pixley. *Critical Properties of Weak Measurement Induced Phase Transitions in Random Quantum Circuits*. 2024. arXiv: [2404.02968](https://arxiv.org/abs/2404.02968) [quant-ph].
- [24] A. Altland et al. “Dynamics of measured many-body quantum chaotic systems”. In: (2021). DOI: [10.48550/ARXIV.2112.08373](https://doi.org/10.48550/ARXIV.2112.08373). URL: <https://arxiv.org/abs/2112.08373>.
- [25] Wojciech H. Zurek. *Decoherence and the transition from quantum to classical – REVISITED*. 2003. arXiv: [quant-ph/0306072](https://arxiv.org/abs/quant-ph/0306072) [quant-ph].
- [26] Wojciech Hubert Zurek and Juan Pablo Paz. “Decoherence, chaos, and the second law”. In: *Phys. Rev. Lett.* 72 (16 Apr. 1994), pp. 2508–2511. DOI: [10.1103/PhysRevLett.72.2508](https://doi.org/10.1103/PhysRevLett.72.2508). URL: <https://link.aps.org/doi/10.1103/PhysRevLett.72.2508>.
- [27] Peter E Kloeden and Eckhard Platen. *Numerical Solution of Stochastic Differential Equations*. Berlin: Springer, 1992.

- [28] L. Onsager and S. Machlup. “Fluctuations and Irreversible Processes”. In: *Phys. Rev.* 91 (6 Sept. 1953), pp. 1505–1512. DOI: [10.1103/PhysRev.91.1505](https://doi.org/10.1103/PhysRev.91.1505). URL: <https://link.aps.org/doi/10.1103/PhysRev.91.1505>.
- [29] S. Machlup and L. Onsager. “Fluctuations and Irreversible Process. II. Systems with Kinetic Energy”. In: *Phys. Rev.* 91 (6 Sept. 1953), pp. 1512–1515. DOI: [10.1103/PhysRev.91.1512](https://doi.org/10.1103/PhysRev.91.1512). URL: <https://link.aps.org/doi/10.1103/PhysRev.91.1512>.
- [30] Claude Cohen-Tannoudji, Bernard Diu, and Franck Laloe. *Quantum Mechanics*. Vol. 1. Translated from the French by S.R. Hemley, N. Ostrowsky, and C.D. Batista. New York: Wiley, 1977. ISBN: 978-0471164333.
- [31] H. J. Carmichael. “Quantum trajectory theory for cascaded open systems”. In: *Phys. Rev. Lett.* 70 (15 Apr. 1993), pp. 2273–2276. DOI: [10.1103/PhysRevLett.70.2273](https://doi.org/10.1103/PhysRevLett.70.2273). URL: <https://link.aps.org/doi/10.1103/PhysRevLett.70.2273>.
- [32] Jean Dalibard, Yvan Castin, and Klaus Mølmer. “Wave-function approach to dissipative processes in quantum optics”. In: *Phys. Rev. Lett.* 68 (5 Feb. 1992), pp. 580–583. DOI: [10.1103/PhysRevLett.68.580](https://doi.org/10.1103/PhysRevLett.68.580). URL: <https://link.aps.org/doi/10.1103/PhysRevLett.68.580>.
- [33] H M Wiseman. “Quantum trajectories and quantum measurement theory”. In: *Quantum and Semiclassical Optics: Journal of the European Optical Society Part B* 8.1 (Feb. 1996), pp. 205–222. DOI: [10.1088/1355-5111/8/1/015](https://doi.org/10.1088/1355-5111/8/1/015). URL: <https://doi.org/10.1088/1355-5111/8/1/015>.
- [34] H.M. Wiseman and G.J. Milburn. *Quantum Measurement and Control*. Cambridge University Press, 2010. ISBN: 9780521804424. URL: <https://books.google.com.br/books?id=ZNjvHaH8qA4C>.
- [35] Todd A. Brun. “A simple model of quantum trajectories”. In: *American Journal of Physics* 70.7 (July 2002), pp. 719–737. DOI: [10.1119/1.1475328](https://doi.org/10.1119/1.1475328). URL: <https://doi.org/10.1119/1.1475328>.
- [36] Kurt Jacobs and Daniel A. Steck. “A straightforward introduction to continuous quantum measurement”. In: *Contemporary Physics* 47.5 (Sept. 2006), pp. 279–303. ISSN: 1366-5812. DOI: [10.1080/00107510601101934](https://doi.org/10.1080/00107510601101934). URL: <http://dx.doi.org/10.1080/00107510601101934>.

- [37] Klaus Mølmer, Yvan Castin, and Jean Dalibard. “Monte Carlo wave-function method in quantum optics”. In: *J. Opt. Soc. Am. B* 10.3 (Mar. 1993), pp. 524–538. DOI: [10.1364/JOSAB.10.000524](https://doi.org/10.1364/JOSAB.10.000524). URL: <https://opg.optica.org/josab/abstract.cfm?URI=josab-10-3-524>.
- [38] Francesco Ciccarello et al. “Quantum collision models: Open system dynamics from repeated interactions”. In: *Physics Reports* 954 (Apr. 2022), pp. 1–70. ISSN: 0370-1573. DOI: [10.1016/j.physrep.2022.01.001](https://doi.org/10.1016/j.physrep.2022.01.001). URL: <http://dx.doi.org/10.1016/j.physrep.2022.01.001>.
- [39] Michael A. Nielsen and Isaac L. Chuang. *Quantum Computation and Quantum Information: 10th Anniversary Edition*. Cambridge University Press, 2011. ISBN: 9781107002173. URL: <https://www.amazon.com/Quantum-Computation-Information-10th-Anniversary/dp/1107002176?SubscriptionId=AKIAIOBINVZYXZQZ2U3A&tag=chimbori05-20&linkCode=xm2&camp=2025&creative=165953&creativeASIN=1107002176>.
- [40] U. Weiss. *Quantum Dissipative Systems*. G - Reference, Information and Interdisciplinary Subjects Series. World Scientific, 2012. ISBN: 9789814374910. URL: <https://books.google.com.br/books?id=qgfuFZxvGKQC>.
- [41] M.E.J. Newman. *Computational Physics*. CreateSpace Independent Publishing Platform, 2013. ISBN: 9781480145511. URL: <https://books.google.com.br/books?id=SS6uNAECAAJ>.
- [42] John Preskill. *Lecture Notes for Ph219/CS219: Quantum Information and Computation*. California Institute of Technology. Updated annually (originally published in 1998). 2022.
- [43] H.M. Nussenzveig. *Curso de física básica: Ótica, relatividade, física quântica (vol. 4)*. BLUCHER, 2014. ISBN: 9788521208044. URL: <https://books.google.com.br/books?id=utSsDwAAQBAJ>.
- [44] Richard P. Feynman. “Space-Time Approach to Non-Relativistic Quantum Mechanics”. In: *Reviews of Modern Physics* 20.2 (1948), pp. 367–387. DOI: [10.1103/RevModPhys.20.367](https://doi.org/10.1103/RevModPhys.20.367).
- [45] A. Altland and B. Simons. *Condensed Matter Field Theory*. New York: Cambridge University Press, 2010.

- [46] Leticia F Cugliandolo and Vivien Lecomte. “Rules of calculus in the path integral representation of white noise Langevin equations: the Onsager–Machlup approach”. In: *Journal of Physics A: Mathematical and Theoretical* 50.34 (July 2017), p. 345001. DOI: [10.1088/1751-8121/aa7dd6](https://doi.org/10.1088/1751-8121/aa7dd6). URL: <https://dx.doi.org/10.1088/1751-8121/aa7dd6>.
- [47] Herbert Goldstein, Charles P. Poole, and John L. Safko. *Classical Mechanics*. 3rd. Reading, MA: Addison-Wesley, 2001. ISBN: 978-0201657029.
- [48] Don S. Lemons and Anthony Gythiel. “Paul Langevin’s 1908 paper “On the Theory of Brownian Motion” [“Sur la théorie du mouvement brownien,” C. R. Acad. Sci. (Paris) 146, 530–533 (1908)]”. In: *American Journal of Physics* 65.11 (Nov. 1997), pp. 1079–1081. ISSN: 0002-9505. DOI: [10.1119/1.18725](https://doi.org/10.1119/1.18725). eprint: [https://pubs.aip.org/aapt/ajp/article-pdf/65/11/1079/12107627/1079\1\\_online.pdf](https://pubs.aip.org/aapt/ajp/article-pdf/65/11/1079/12107627/1079\1_online.pdf). URL: <https://doi.org/10.1119/1.18725>.
- [49] C.W. Gardiner. *Handbook of Stochastic Methods for Physics, Chemistry, and the Natural Sciences*. Proceedings in Life Sciences. Springer-Verlag, 1985. ISBN: 9780387113579. URL: <https://books.google.com.br/books?id=cRfvAAAAAAAJ>.
- [50] Abraham Pais. *Subtle is the Lord: The Science and the Life of Albert Einstein: The Science and the Life of Albert Einstein*. Oxford University Press, USA, 1982.
- [51] Hiroshi Kunita. “Itô’s stochastic calculus: Its surprising power for applications”. In: *Stochastic Processes and their Applications* 120.5 (2010). A tribute to Kiyosi Itô, pp. 622–652. ISSN: 0304-4149. DOI: <https://doi.org/10.1016/j.spa.2010.01.013>. URL: <https://www.sciencedirect.com/science/article/pii/S0304414910000220>.
- [52] N.G. Van Kampen. *Stochastic Processes in Physics and Chemistry*. North-Holland Personal Library. Elsevier Science, 2011. ISBN: 9780080475363. URL: <https://books.google.com.br/books?id=N6II-6H1PxEC>.